FINAL REPORT

AN INVESTIGATION OF CONDENSATION HEAT TRANSFER
IN A CLOSED TUBE CONTAINING A SOLUBLE
NONCONDENSABLE GAS

Grant No. NSG-2015

by

Elric W. Saaski

and

Richard J. Hanson
Associate Professor, Computer Science Dept.
Washington State University
Pullman, Washington   99163

TABLE OF CONTENTS

ii

LIST OF FIGURES

iii

1.0 INTRODUCTION

The condensation of vapor on the inside surface of a tube is an important heat transfer mechanism in many thermal devices. An example of such a device is the heat pipe. This is a liquid-vapor two-phase system, often in the form of a closed tube, which transfers heat by evaporation and condensation at opposing ends of the tube. The heat pipe has been used to advantage in many aerospace and satellite systems, and is now being recognized as a potentially attractive heat transfer device for terrestrial applications. The intentional or accidental introduction of noncondensable gases into heat pipes significantly changes the condensation heat transfer characteristics of the heat pipe condenser. This unique behavior has been widely used for temperature control in gas-loaded heat pipes. This report describes experiments and analyses done to further establish the characteristics of these gas zones in the limit as the gas becomes increasingly soluble in the working fluid.

Early analyses of the gas-controlled heat pipe assumed a very simple model for position and effect of noncondensable gas within the condenser; that is, the noncondensable gas was assumed to be in the form of a plug with a sharply-defined vapor-gas interface. In time it was found that the flat-front model did not accurately represent many systems. It was observed that axial heat transfer via the condenser wall caused the sharp front to become more diffuse and that the boundary was also elongated due to vapor diffusion into the stagnant gas zone. The culmination of one-dimensional models including wall conduction was the numerical program GASPIPE[1] which allowed the user flexibility in modeling condenser heat transfer effects and yielded better agreement between design calculations and experimental observation.

In this study a more exact one-dimensional condensation heat transfer model for insoluble gases has been developed and compared with experimental data. Modifications to this model to accommodate soluble gas behavior have also been accomplished, and the effects on gas front behavior demonstrated.

In Section 2, Analysis, analytical models for condensation heat transfer are documented. In Section 3, Experimental Apparatus and Technique, a novel optical method used for measuring gas concentration profiles is outlined. Section 3 also presents experimental data. Section 4 is an interpretation of these data and Section 5 is the summary and conclusion.

2.0 ANALYSIS

In this section models are developed for condensation heat transfer and dissolved gas transport in a gas-loaded heat pipe. The influence on condensation of an insoluble noncondensable gas is developed in Section 2.1, while various effects of a soluble gas are explored in Section 2.2. The intention of these sections is to construct an analytical framework that can be used for comparison with experimental heat transfer data presented in Section 3.8, Experimental Results.

2.1 One-dimensional Model for Condensation in the Presence of an Insoluble Noncondensable Gas

To determine the effect of gas solubility on condensation heat transfer in a heat pipe, it is worthwhile to develop an analytical model for condensation in the presence of an insoluble gas so that a bench mark or reference model is available for comparison with data. An additional incentive for developing such a model evolved during execution of this study--the soluble gas models, in addition to being complex, were numerically unstable. These problems are discussed in more detail in Section 2.2, Soluble Gas Modeling.

The coupled heat transfer and mass transfer processes in the condenser have been described by two one-dimensional conservation equations accounting for heat and mass transfer in the vapor phase and heat transfer along and through the heat pipe wall. Both axial and radial pressure gradients are neglected, and composition and temperature are assumed uniform across the entire vapor cross section. The boundary conditions used are similar to those of Marcus,[1] but certain simplifying assumptions have not been made. Specifically, the first and second spatial derivatives for vapor and wall temperature are not assumed equal, allowing accurate representation of high thermal

resistance systems such as the glass heat pipe used in experimental phases of this study. The modeling described in this section is similar to modeling by Saaski,[2] but various improvements have been incorporated which increase solution accuracy and reduce computational time.

2.1.1 Vapor Phase Mass Transfer

The intent of this modeling is to define heat transfer in the stagnant gas zone shown in Figure 2.1 and existing between the axial positions $z_0 \leq z \leq z_m$. A cylindrical heat pipe cross section is assumed, but the equations to be developed are not geometry-dependent. However, uniform wall and vapor cross-sectional areas are necessary. An immiscible gas/fluid combination is also assumed. If axial and radial pressure gradients and thermal conduction are negligible in the vapor phase, and the heat pipe wall is uniform in temperature along any circumferential line, then vapor migration into the gas zone can be modeled as diffusive flow into a stagnant gas layer. Conservation of working fluid vapor (species a) at any cross section results in the coupled heat and mass transfer equation

$$\frac{d\phi_a}{dz} = \frac{G_f(T_v - T_w)}{A_v H_{fg}} \tag{2-1}$$

where ϕ denotes molar flux and T_v and T_w represent the vapor and wall temperatures respectively. H_{fg} is the molar heat of vaporization and the vapor cross-sectional area is A_v. This expression is based on the vapor phase being separated from the wall by a liquid film of uniform conductance per unit length, G_f. This constant thickness film is attributable to a uniform thickness capillary wick upon the wall. In the case of reflux operation without a wick, the film thickness is a slowly varying function of axial position, but can often
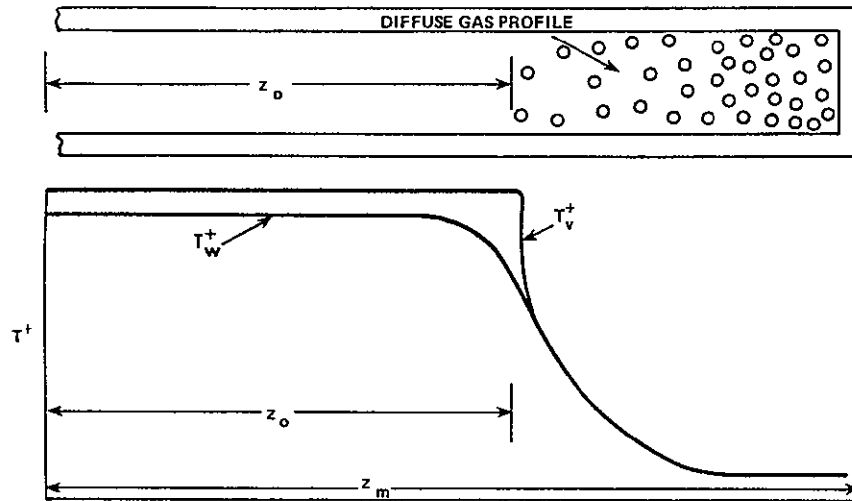
FIGURE 2.1. REPRESENTATIVE THERMAL PROFILES FOR A GAS-LOADED HEAT PIPE

be approximated by a constant value. The surface of this film which is in contact with the vapor phase is at the vapor phase temperature; any interfacial resistances are assumed small. For an insoluble gas, there is no net gas movement and $\phi_b = 0$ (b denotes the noncondensable gas). The molar flux of species a is given as

$$\phi_a = \frac{CD_{ab}dX_a/dz}{(1 - X_a)} \tag{2-2}$$

so that

$$\frac{d}{dz}\left(\frac{CD_{ab}dX_a/dz}{1 - X_a}\right) = \frac{G_f(T_v - T_w)}{A_v H_{fg}} \tag{2-3}$$

The ultimate goal is to obtain a differential equation which has T_v as the primary dependent variable. With this objective in mind, the mole fraction X_a in a constant pressure system is expressible as

$$X_a = \frac{P_s}{P_{sm}} \tag{2-4}$$

and

$$P_s = f(T_v); \quad \frac{dP_s}{dT_v} = F'; \quad \frac{d^2P_s}{dT_v^2} = F'' \tag{2-5}$$

where P_s is a function of the vapor temperature T_v, and P_{sm} is the total heat pipe internal pressure. The concentration-diffusivity product, CD_{ab}, can be expressed as a function of T_v through the Chapman-Enskog formula for dilute gases

$$CD_{ab} = B \sqrt{T_v} \tag{2-6}$$

where B is a very slowly varying function of temperature, and T_v is expressed in absolute temperature. For practical purposes, B can be evaluated at a mean temperature and assumed to be a constant.

When the expressions above are substituted into equation (2-3), a second-order nonlinear differential equation in T_v results

$$\frac{d^2T_v}{dz^2} + \left[\frac{f''}{f'} + \frac{f'}{X_b P_{sm}} + \frac{1}{2T_v}\right]\left(\frac{dT_v}{dz}\right)^2 = \frac{G_f X_b P_{sm}}{f' A_v H_{fg} CD_{ab}} \cdot \left(T_v - T_w\right) \tag{2-7}$$

The numerical technique used to solve this equation is discussed in Section 2.1.3.

2.1.2 Axial Wall Conduction

The heat pipe wall is assumed uniform in cross section and to have a temperature dependence on the z-coordinate only. The wall is coupled to the vapor phase through a film or layer with per-unit-length thermal conductance G_f and to the heat sink through a similar conductance, G_i. In Figure 2.2, this series of thermal conductances is shown as both a nodal network and as related to the condenser-heat sink assembly. A steady-state heat balance on an infinitesimal wall slice leads to the differential equation used in the experimental phase of this study:

$$\frac{d^2T_w}{dz^2} = \frac{1}{A_w K_w} \left(G_i(T_w - T_s) - G_f(T_v - T_w) \right) \tag{2-8}$$

where T_s is the heat sink temperature and A_w and K_w are the wall cross-sectional area and thermal conductivity.

2.1.3 Numerical Solution Method - One-dimensional Problem

In the last two sections, second-order differential equations for T_v and T_w have been derived. Under steady-state operating conditions, both equations must be satisfied simultaneously at all axial positions.

By formation of a nodal network as shown in Figure 2.2, it has been possible to solve the coupled equations (2-7) and (2-8) by converting the equations to finite difference form and using successive over-relaxation (SOR) to iteratively approach consistent profiles for T_v and T_w. However, the approach has required long computational times and alternate methods for solving the equations were investigated. All failed but one. Most notable among the failures was the so-called "shooting technique" in which initial guesses for the temperatures and their derivatives at $z = z_o$ are adjusted until the

SYSTEM COMPONENT	DESIGNATION
VAPOR TEMPERATURE	T_v
FLUID FILM CONDUCTANCE	G_f
WALL TEMPERATURE	T_w
INTERFACIAL CONDUCTANCE	G_i
HEAT SINK	T_s

EQUIVALENT FINITE DIFFERENCE NODAL NETWORK
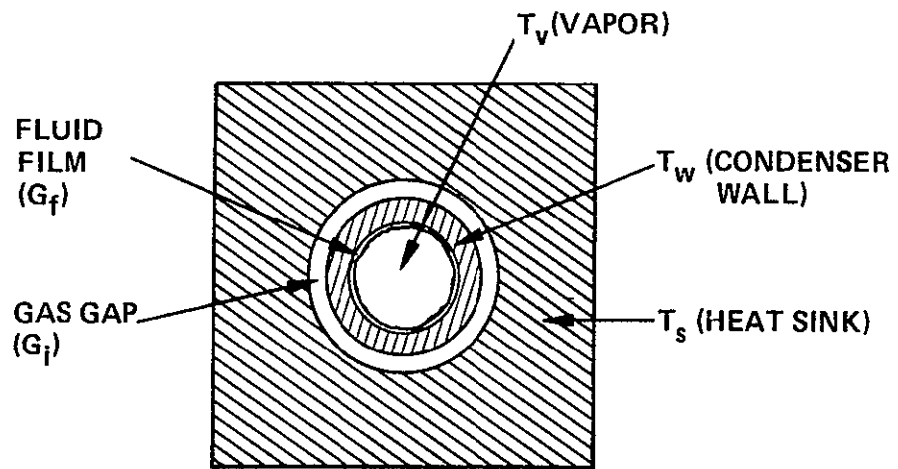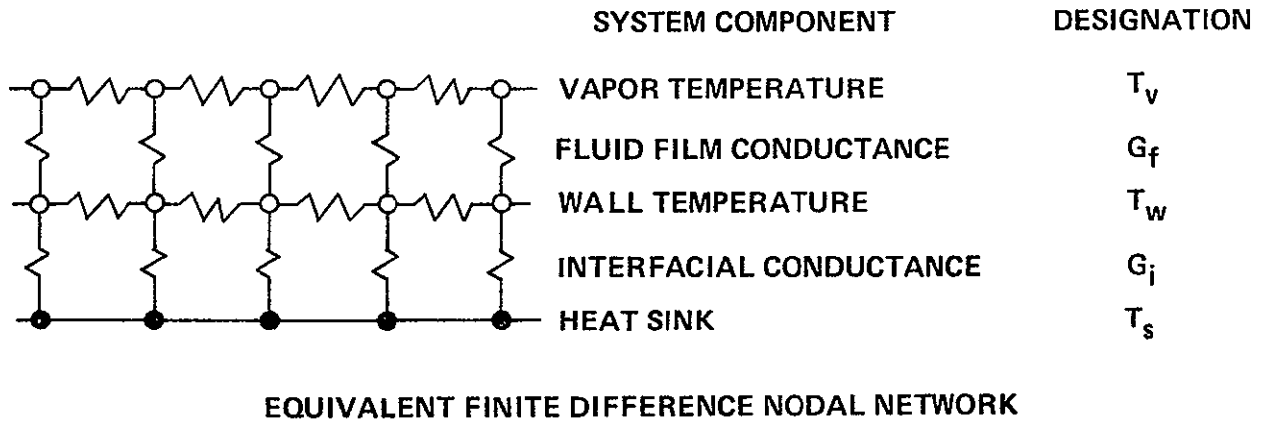
CROSS SECTION OF
HEAT REJECTION ASSEMBLY

FIGURE 2.2.   FINITE DIFFERENCE MODEL FOR GAS-GAP CONDENSER/HEAT SINK ASSEMBLY

solutions at $z = z_m$, obtained by integrating the differential equations across the zone, satisfy a zero derivative boundary condition at z_m. However, the solution for T_v would invariably either rise or fall with great speed after a number of apparently stable increments in z. The nonlinear equation (2-7) has many of the mannerisms of a "stiff" equation.

Successive over-relaxation is commonly employed as a point-iterative technique; that is, one point at a time is adjusted in value. A block relaxation technique was defined which was stable and improved convergence rates. Taken individually, the finite difference forms of (2-7) and (2-8) are tridiagonal matrices for T_{vi} and T_{wi}, if temperatures on the other nodal line are fixed. That is, in the nodal network of Figure 2.2, if the wall temperatures are held fixed at one iterative step, then the system of linear equations defining the axial vapor temperature profile is tridiagonal. A tridiagonal matrix can be solved exactly using the Thomas algorithm.[3] This exact set of vapor temperatures is then held constant, and a new line of wall temperatures is calculated using the Thomas algorithm. The new wall temperatures are held constant and a vapor profile is calculated again as in the first step, completing the iterative cycle. All theoretical profiles were generated using this block iterative technique.

Prior to generating difference equations, the temperatures and axial coordinate system were nondimensionalized as follows:

$$T^+ = \frac{T-T_s}{T_m-T_s} \; ; \qquad z^+ = \sqrt{\frac{G_i z^2}{A_w K_w}} \tag{2-9}$$

where T_m is the adiabatic vapor temperature. The vapor pressure $f(T_v)$ was found by fitting experimental vapor pressure data to the following form:

$$\ln f = a_o + a_2/T_v + a_3 \ln(T_v) \qquad (2\text{-}10)$$

The vapor temperature T_v is in absolute degrees. The finite difference form of equation (2-7) can be configured into a tridiagonal matrix with each row given by

$$\alpha_i \ T^+_{v,\ i-1} + \beta_i \ T^+_{v,i} + \gamma_i \ T^+_{v,i+1} = d_i \qquad (2\text{-}11)$$

For intermediate points excluding the boundaries, the constants are defined by the following set of equations:

$$\alpha_i = 1 - E_i \qquad (2\text{-}12)$$

$$\beta_i = -(2 + F_i) \qquad (2\text{-}13)$$

$$\gamma_i = 1 + E_i \qquad (2\text{-}14)$$

$$E_i = \left(\frac{T_m - T_s}{4\ T_{v,i}}\right) \left(T^+_{v,i+1} - T^+_{v,i-1}\right) \left[\frac{U}{1-X_a} + \frac{a_2}{U\ T_{v,i}} - \frac{1}{2}\right] \qquad (2\text{-}15)$$

$$U = a_3 - a_2/T_{v,i} \qquad (2\text{-}16)$$

$$F_i = \frac{B\ T_{v,i}}{U} \left(\frac{1}{X_a} - 1\right) \left(\Delta z^+\right)^2 \qquad (2\text{-}17)$$

$$B = \left(\frac{G_f}{G_i}\right)\left(\frac{A_w}{A_v}\right)\left(\frac{K_w}{CD_{ab}H_{fg}}\right) \qquad (2\text{-}18)$$

$$d_i = F_i \bullet T^+_{w,i} \qquad (2\text{-}19)$$

The finite difference equations for the wall were similarly derived and will not be presented. Boundary conditions used in modeling were

$$T_v^+ = 1.0 \qquad z^+ < z_o^+ \qquad (2\text{-}20)$$

$$T_v^+ = 0.995 \qquad z^+ = z_o^+ \qquad (2\text{-}21)$$

$$T_w^+ = 1/(1 + G_i/G_f) \qquad z^+ = z_o^+ - 0.75 \qquad (2\text{-}22)$$

$$\cdot \quad \frac{dT_w^+}{dz^+} = \frac{dT_v^+}{dz^+} = 0 \qquad z^+ = z_o^+ + 8.5 \qquad (2\text{-}23)$$

Standard methods were used to incorporate these boundary conditions into the finite difference equation sets; for example, the derivative boundary conditions were expressed as central divided differences.

The dimensionless vapor temperature was calculated over the range $z_o^+ < z^+ \leq z_o^+ + 8.5$. At a distance of 8.5 dimensionless units from the gas front, the gas concentration is essentially constant and calculations over a longer zone are not necessary and reduce solution accuracy in the area around z_o^+ for a fixed number of increments. The axial gas zone was divided into 114 increments. Wall temperatures were calculated over a wider range extending into the nonblocked condenser zone. This is done because the heat pipe wall in the gas zone acts as an extended fin, draining heat away from the warmer areas and depressing wall temperature beyond the actual gas front.

A listing of the computer program used for modeling purposes is given in Appendix C. The code is in BASIC language and was programmed on a PDP-11 minicomputer. Representative profiles are tabulated in Appendix B, and a comparison with experimental data is given in Figure 3.10. Iteration of temperature profiles was terminated when the largest change in wall

temperature per iteration was less than 0.001 in dimensionless units. This typically required 40 iterations—at the end of these iterations, the vapor temperature was often very slightly less than the wall temperature for $z^+ \gg z_0^+$. With a larger number of iterations this physically unrealistic situation is corrected, but the difference in profile shapes is quite negligible, and was not considered worth the additional computer run-time. Forty iterations required about 5 to 6 minutes of CPU time on the PDP-11.

2.2 Soluble Gas Modeling

An initial attempt to model condensation in a tube containing soluble gas was done using a von Karman-Pohlhausen integral technique. By assuming characteristic equations for the concentration and velocity profiles in both vapor and liquid phases, it was possible to generate coupled differential equations describing the two-dimensional concentration and flow fields for incompressible flow. The approach used was similar to that of Somogyi and Yen.[4] The analysis developed will not be presented here in detail because the authors were unsuccessful in obtaining stable numerical solutions.

A shooting technique was used from the interface at $z = z_0$. A stable solution set was obtained until the differential integration approached the fully stagnant gas plug zone. Under these conditions, the fluid film on the heat pipe wall is saturated with a large amount of noncondensable gas, and the gas-saturated liquid moves toward the evaporator into regions of lower vapor-phase gas concentration. This supersaturation creates a large gas flux out of the fluid surface and, in fact, the integral techniques indicated total vapor phase fluxes that were directed radially inward. When this occurred, the solution became unstable and was not correctable with smaller steps in z. Because of these large radially inward gas fluxes, it was not

possible to obtain a zero derivative for concentration and zero value for the axial and radial velocity components at $z = z_m$. The integral method was abandoned and the hybrid 1D/2D method described in the following section was developed.

2.2.1 Hybrid Soluble Gas Model

For tubes on the order of 1 cm diameter and vapor pressures of 1 atmosphere (typical heat pipe conditions), vapor phase diffusivity can be much higher than liquid phase diffusivity. Vapor phase diffusivities range typically from 0.1 to 1.0 cm^2/sec, while liquid phase diffusivities of 1 to 10×10^{-5} cm^2/sec are typical for gases in common working fluids.

Therefore, if radial concentration gradients are neglected in the vapor phase but are accounted for in the liquid phase, it is possible to extend the analysis of Section 2.1 to include soluble gas effects for a wide range of physically relevant heat pipe designs.

If interfacial resistance is neglected at the vapor/liquid interface as in Section 2.1, then the concentration of gas at the liquid phase interface is in the equilibrium with the gas concentration in the vapor phase, and

$$C_{g\ell} = \alpha\, C_{gv} \qquad \text{(at liquid/vapor interface)} \qquad (2\text{-}24)$$

where $C_{g\ell}$ is the liquid phase gas concentration, C_{gv} is the vapor phase gas concentration, and α is the Ostwald coefficient. A mass balance on the working fluid vapor yields the same expression as equation (2-1). However, the noncondensable gas is no longer stationary, and the equation (2-2) for ϕ_a must be modified to

$$\phi_{as} = \frac{X_a \phi_b - CD_{ab} X_a/dz}{1 - X_a}$$

(2-25)

and the conservation equation for coupled heat transfer and vapor transfer is

$$\frac{d}{dx} (\phi_{as}) = \frac{G_f(T_v - T_w)}{A_v H_{fg}}$$

(2-26)

To obtain the flux ϕ_b in (2-25), transport of noncondensable gas within the surface liquid layer must be detailed. In the experiments described in Section 3, the heat pipe was wickless and vertically oriented with the evaporator at the bottom. The surface layer therefore is in the classic falling film category as investigated by Nusselt and others. If it is assumed that the dissolved gas has no effect on physical properties of the liquid and that diffusion of dissolved gas in the vertical direction is negligible compared to convective transport, then conservation of gas in the film is governed by

$$V(y,z) \frac{\partial C_g}{\partial z} = D_\ell \frac{\partial^2 C_{g\ell}}{\partial y^2}$$

(2-27)

where $V(y,z)$ is the film velocity and D_ℓ is the diffusion coefficient of the gas in the liquid. The coordinate y is measured radially inward with respect to the heat pipe inner wall surface.

Under conditions of laminar flow, negligible shear at the liquid-vapor interface, and negligible vapor density compared to liquid density, the velocity profile is

$$V(y^+) = \frac{\rho_\ell g \delta^2}{\mu_\ell} \cdot \left(y^+ - 1/2 y^{+2} \right)$$

(2-28)

where $\quad y^+ = y/\delta$ $\hspace{4cm}$ (2-29)

The fluid density and viscosity are ρ_ℓ and μ_ℓ, respectively. The fluid film thickness is δ. At the wall, $V(0)$ is zero, while at the vapor/liquid interface, $V(1)$ is a maximum.

Boundary conditions on C_g are

$$C_{g\ell} = \alpha C_{gv} \hspace{3cm} y^+ = 1 \hspace{3cm} (2\text{-}30)$$

$$\frac{dC_{g\ell}}{dy} = 0 \hspace{3cm} y^+ = 0 \hspace{3cm} (2\text{-}31)$$

$$C_{g\ell} = \alpha C_{gvm} \hspace{2.5cm} z = z_m, \ 0 \ y^+ \ 1 \hspace{1.5cm} (2\text{-}32)$$

At $z = z_m$, the dissolved gas concentration has reached a maximum value in equilibrium with the fully stagnant gas concentration, C_{gvm}.

The liquid film thickness δ changes with axial position because of condensation. By using the velocity distribution (2-28) and assuming a linear temperature profile across the film, film growth is obtained by integrating over the heat transferred from $z = z_1$ to $z = z_m$, where $z_0 \ z_1 \ z_m$. The film thickness δ is given by

$$\frac{t_w \delta^3}{6 K_w} + \frac{1}{4} \frac{\delta^4}{K_\ell} = \frac{M_a}{2 g H_{fg}} \int_{z_1}^{z_m} (T_v - T_w) \, dz \hspace{2cm} (2\text{-}33)$$

where t_w is the heat pipe wall thickness.

For coupling to the finite difference equations it was necessary to include the wall thermal resistance between the fluid film and the node at the center of the wall. For metal-walled heat pipes this radial wall

temperature drop can be neglected, but it is of first-order importance in a glass heat pipe because of a much lower thermal conductivity.

For numerical solution of the conservation equation (2-27), a dimensionless gas concentration and radial measure were defined.

$$c^+ = \frac{C_{g\ell}}{\alpha C_{gvm}} \quad ; \quad y^+ = \frac{y}{\delta} \tag{2-34}$$

The gradually-changing film width δ must be accounted for in the conservation equation

$$V(y^+,z) \bullet \left(\frac{\partial c^+}{\partial z} - \frac{y^+}{\delta} \bullet \frac{d\delta}{dz} \bullet \frac{\partial c^+}{\partial y^+} \right) = \frac{D_\ell}{\delta^2} \frac{\partial^2 c^+}{\partial y^{+2}} \tag{2-35}$$

The conservation equation (2-35) with boundary conditions 2-30 through 2-32 was solved by implicit finite difference methods similar to those described in Section 2.1. The gas phase concentrations C_{gv} used in boundary conditions 2-30 were obtained from a finite difference solution of the vapor phase equation (2-26). This solution was also obtained in a manner entirely analogous to the solution method in Section 2.1 except for inclusion of the new term in ϕ_a, i.e.,

$$\text{new term} = \frac{x_a}{1-x_a} \phi_b \tag{2-36}$$

The axially-varying flux ϕ_b was obtained from the solution to the liquid-phase diffusion problem. At each axial position, a mass balance including both the vapor and liquid phases shows that the flux $A_v \phi_b$ in the vapor phase must be balanced by a gas flux of opposite sign within the liquid phase.

The liquid-phase gas flux $A_\ell \phi_{b\ell}$ is obtained by numerically integrating the concentration profile,

$$A_\ell \phi_{b\ell} \bigg|_{z=z_1} = \alpha \pi D_\ell \delta \; C_{gvm} \int_0^1 V(y^+) \cdot c^+ dy^+ \qquad (2\text{-}37)$$

where D_ℓ is the heat pipe inner diameter.

The coupled problem was iteratively solved by alternately holding the solution fixed in one phase and solving the finite difference equation in the other phase. At the completion of each cycle, $\phi_b(z)$ would be updated. When the concentration profiles in each phase remained constant with iteration, the coupled problem was considered solved.

3.0 EXPERIMENTAL APPARATUS AND TECHNIQUE

3.1 Alternate Methods for Measuring Vapor Phase Gas Concentration

To compare experimental data with analytical models for condensation in the presence of a soluble gas, an approach is desired which indicates accurately both vapor phase composition and spatial variations in composition. Many previous investigators have inferred internal vapor phase dynamics from variations in heat pipe wall temperature, or from probe temperatures in the vapor phase. The first method has the obvious deficiency of not being a direct measurement and, in fact, it is easy to show that measured axial temperature variations are primarily related to axial wall conduction for most metal-walled heat pipes. It is very difficult to infer from external measurements an accurate picture of vapor phase mass transfer in the transition zone between the freely condensing and fully stagnant zones.

It is also difficult to accurately measure the condition of the vapor phase directly. Any probe inserted into the vapor generally has such a large thermal mass that profiles can be severely distorted. Thermocouple techniques or thermistors are generally difficult to integrate into an operating heat pipe, not only affecting the accuracy of temperature measurement through their own mass, but also fundamentally changing the flow distribution.

If a small diameter thermocouple well is placed along the axis of a cylindrical heat pipe, boundary conditions for the Navier-Stokes equations are modified as:

$$\text{BEFORE PROBE:} \qquad \text{at } r = 0, \quad U = U_o, \quad \frac{\partial U}{\partial r} = 0$$

$$\text{AFTER PROBE:} \qquad \text{at } r = 0, \quad U = 0, \quad \frac{\partial U}{\partial r} = 0$$

where U represents the axially-directed velocity component. This is a very
fundamental change in velocity distribution and, therefore, the measurement
technique has significantly influenced the system being measured.

3.2 Vapor Composition by Optical Spectroscopy

As discussed, spatial variations in noncondensable gas concentration are
difficult to measure within an operating heat pipe without obtaining a dis-
torted picture of vapor composition. This difficulty has been overcome to a
great extent by using optical spectroscopy.

The basic concept is shown in Figure 3.1. A working fluid/gas combina-
tion is selected in which the noncondensable gas is either strongly absorbent
or optically transparent at a wavelength where the working fluid vapor is of
opposite characteristic. Using a monochromatic light source, such as a laser
or spectrophotometer, the outgoing beam from the source is shaped by a narrow
slit perpendicular to the heat pipe axis. The heat pipe envelope is glass,
and light transmitted through the heat pipe impinges upon a sensitive photo-
cell coupled to a picoammeter. The heat pipe/condenser assembly is mounted
on a vertical drive so that the heat pipe can be scanned by the beam.

Absorption of light by a gas is given by the familiar Lambert-Beer Law

$$I = I_0 \ EXP(-\beta C_b z_{ab}) \tag{3-1}$$

where I_0 is the incident light intensity, β is an absorption coefficient, and
z_{ab} is the distance of light travel through the absorbing medium. C_b is the
effective, geometrically-weighted average concentration along the path at any
given axial position. At constant wavelength a photo-diode has a linear
response to light intensity, so that I and I_0 can also be regarded as photo-
detector current. Therefore, if β and z_{ab} are known, concentration of the
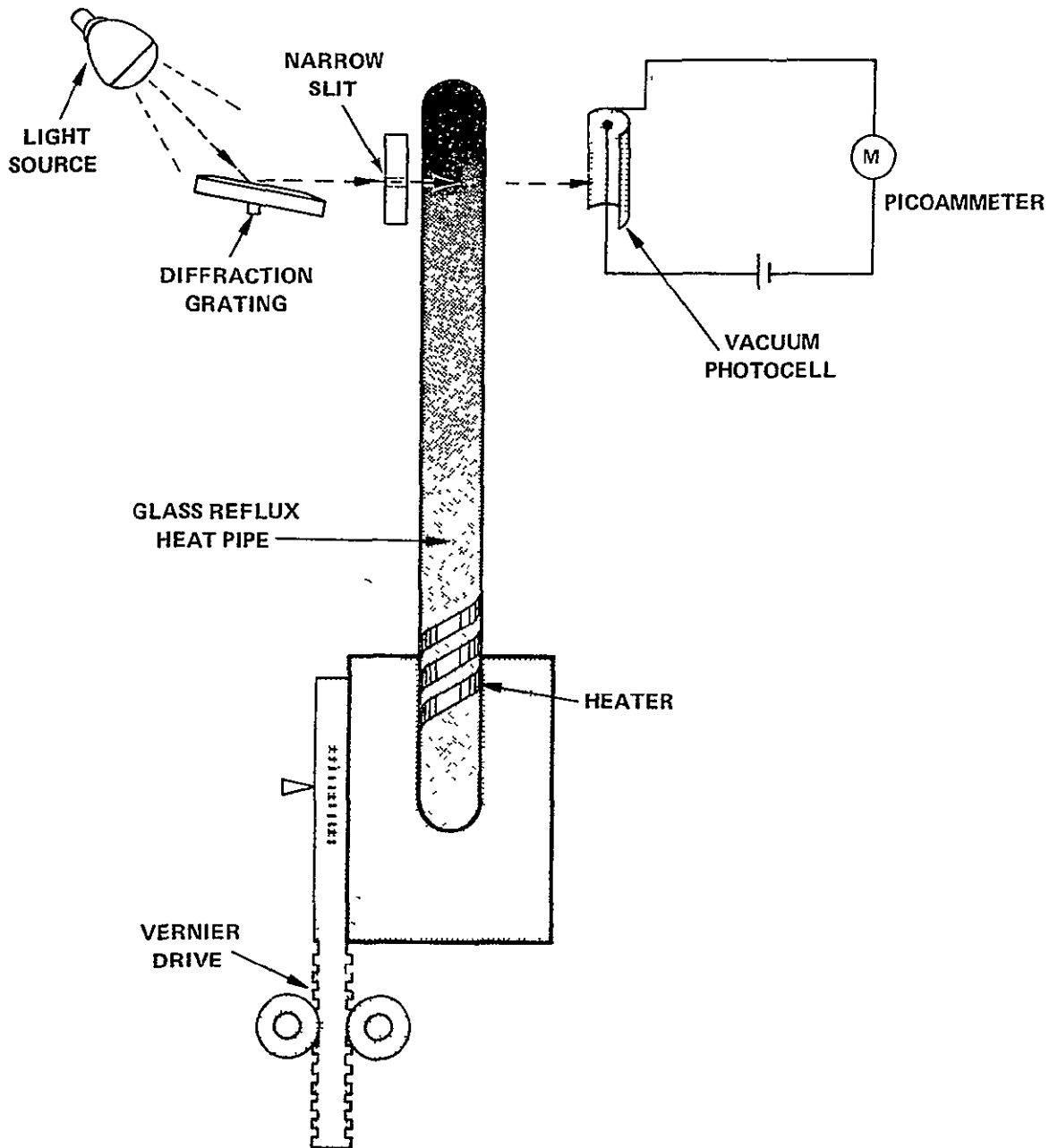
FIGURE 3.1. BASIC TECHNIQUE USED FOR MEASURING CONCENTRATION PROFILES
OF OPTICALLY-ABSORBING GASES IN A REFLUXING TWO-PHASE SYSTEM

absorbing species, C_b, can be found.

$$C_b = \frac{1}{\beta z_{ab}} \ln\left(\frac{I_o}{I}\right) = \frac{I}{\alpha} \ln\left(\frac{I_o}{I}\right) \qquad (3\text{-}2)$$

The constant α now is a cell constant and assumes uniform geometry along the heat pipe length.

This technique allows very accurate measurement of gas concentration versus axial position with minimum disturbance to the heat pipe vapor. Spatial variation along the heat pipe axis can be defined to any degree of accuracy by decreasing slit width, although practical limits arise in obtaining adequate light intensity to drive the photodetector.

The technique also has some limitations. It is obvious that the technique is principally useful in defining the average concentration as a function of axial position; the beam in effect integrates any radial variations. It is also not advisable to use any wick upon the heat pipe inner diameter, as it will optically scatter light. Therefore, this technique is most useful for studying condensation in the presence of noncondensable gases upon smooth vertical surfaces. Such surfaces are of considerable importance in two-phase heat transfer equipment; for example, many terrestrial applications use heat pipes in vertical reflux, in exact agreement with the method optimum for testing. In addition, both vapor phase and condensate phase conditions are very similar to conditions in zero-g, where a wall wick and surface tension pumping replace the falling condensate film defined by viscous shear and gravity.

3.3 Apparatus Description

Table 3.1 summarizes the experimental system.

TABLE 3.1. EXPERIMENTAL TEST VEHICLE
CHARACTERISTICS

Heat Sink

Type	Gas-gap chiller block with optical slot; Aluminum
Length	15.24 cm
Diameter	1.4618 ±0.0013 cm (I.D.)
Optical slot width	0.318 cm
Optical slot height	13.20 cm
Heat pipe centering method	Four 6-32 nylon screws at each end of sink
Conductance of centering screws	0.012 W/K for each set of four screws

Heat Pipe

Envelope type	1.395 cm O.D. Pyrex glass tube
Wall thickness	0.12 cm
Nominal length	50.0 cm
Evaporator length	16.0 cm
Adiabatic length	18.8 cm
Working fluid	CCl_4
Gas additive	Chlorine

Optical Assembly

Operating wavelength	3550 Å
Effective beam size at heat pipe	0.10 x 0.318 cm
Nominal indicator current with no absorbing gas	4.03 (10^{-10}) ampere
Background with light source shielded	≤0.02 (10^{-10}) ampere
Resolution	±0.025 (10^{-10}) ampere on 10^{-10} scale

Figures 3.2a and 3.2b present perspective views of the glass heat pipe and aluminum heat sink. The heat sink, which was in the form of a split-shell, had an inner diameter of 1.416 ±0.0013 cm, and was 15.24 cm long. Four cooling channels of 0.63 cm diameter maintained the condenser isothermal. The optical transmission slits were 0.318 cm wide and 13.2 cm long. After the heat sink was machined, it was given a dark brown chromate conversion coating having a high absorptivity in the blue portion of the spectrum. The outside was then painted flat black. In Figure 3.2b, the light beam is visible in the optical slit.

Before operation, the glass heat pipe of 1.345 cm O.D. was inserted into the inner hole, and centrally located using a feeler gauge and 8 radially mounted nylon 6-32 screws; four screws are at the top of the condenser and 4 at the bottom, spaced at 90-degree intervals. These screws served to hold the heat pipe in the condenser with a minimum conductive loss, and establish a uniform gas-gap circumferentially.

The heat pipe was 50 cm in overall length. The evaporator was 16 cm long. To maintain the evaporator and adiabatic sections as thermally isolated as possible, an aluminum walled Dewar, continuously pumped with a nitrogen trap and fore pump, surrounded these sections, and was sealed to the heat pipe at the condenser end with a Buna-N O-ring. Electrical feed-throughs supplied current to the evaporator resistance heater through the opposite end of the Dewar. On the external surface of the Dewar, a uniformly-space resistance heater maintained the exterior of the Dewar within 1°C of the heat pipe adiabatic temperature. This was necessary to reduce thermal losses via the O-ring contact at the condenser end, and via a mounting plate at the opposite end which centrally located the heat pipe in the Dewar. These elaborate precautions were necessary since the heat pipe was operated as much as 75°C above

COOLANT

VERTICAL TRAVERSE
COUPLING BLOCK

THERMOCOUPLE
WELL

OPTICAL SLIT

HEATING TAPE

3/8" INSULATION

ALUMINUM DEWAR WITH
EXTERNAL HEATER TAPE

LUCITE LINE
CONTACT LOW
CONDUCTIVITY SUPPORT

O-RING SEAL

CERAMIC FEED-THROUGH

HEAT PIPE POWER

VACUUM LINE
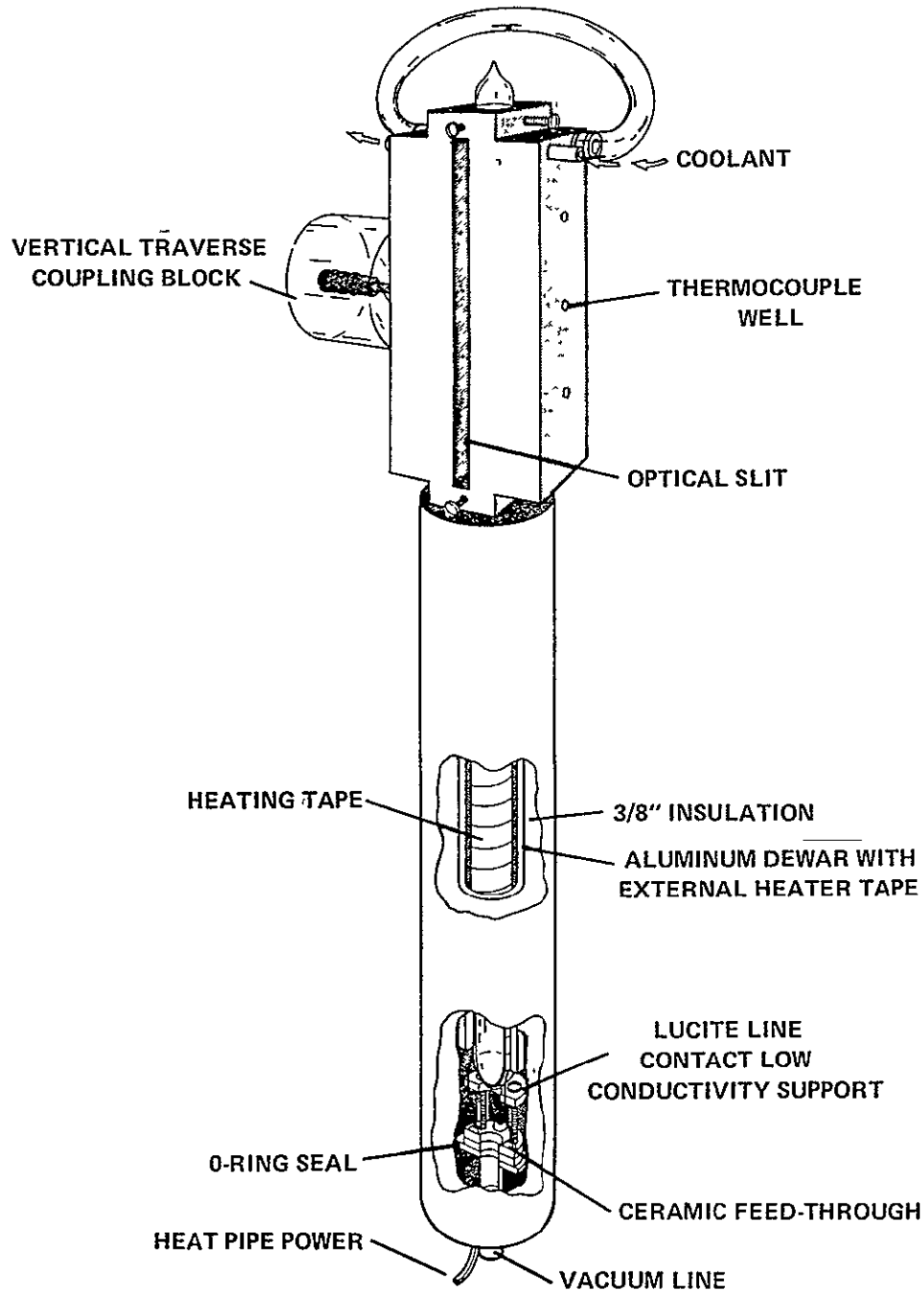
FIGURE 3.2a. PERSPECTIVE VIEW OF TEST SYSTEM USED IN MEASUREMENTS OF AXIAL
NONCONDENSABLE GAS CONCENTRATION DISTRIBUTIONS. BY USING AN
OPTICALLY ABSORBING NONCONDENSABLE GAS, A PRECISE BEAM OF
MONOCHROMATIC LIGHT CAN DEFINE CONCENTRATION PROFILES.
VARIATIONS IN TRANSMITTED LIGHT INTENSITY ARE DIRECTLY RE-
LATED TO CHANGES IN GAS CONCENTRATION

FIGURE 3 2b   FRONTAL VIEW OF CONDENSER AND HEAT SINK SECTIONS
TRANSMITTED LIGHT BEAM IS VISIBLE NEAR THE BOTTOM
OF THE HEAT SINK GROOVE.
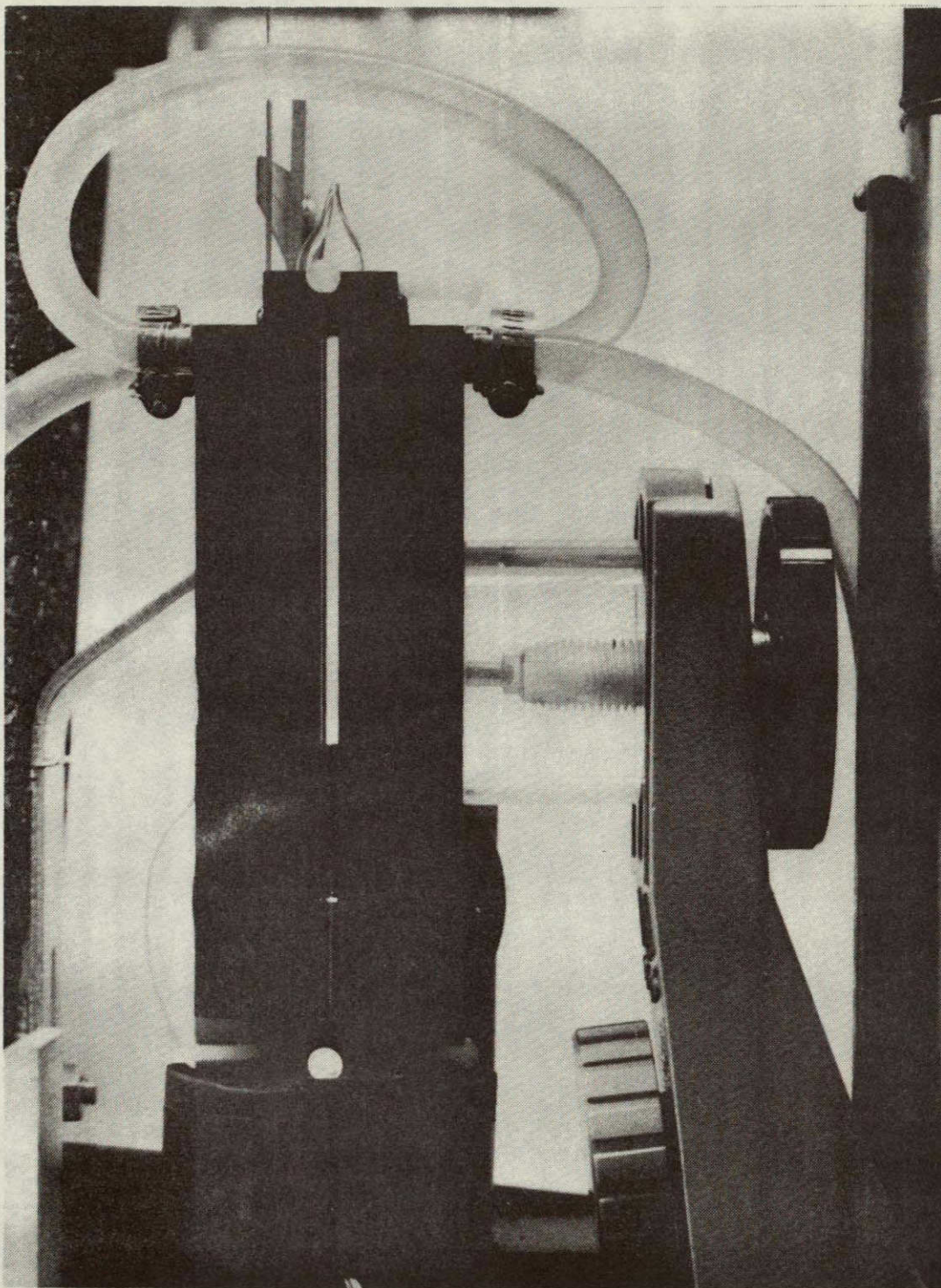
laboratory ambient. The condenser was capable of moving vertically via a friction drive mechanism so that any portion of the transmission slit could be intercepted by the detector beam.

3.4 Gas and Fluid Selection

Based upon a high absorption in the blue spectrum, chlorine was selected as the noncondensable gas. A typical absorption spectrum for Cl_2 gas at 1 atmosphere and $20^{\circ}C$ is shown in Figure 3.3. An operating wavelength of 3550 Å was selected for all optical tests. This wavelength is very close to the absorption peak of Figure 3.3. As a working fluid, carbon tetrachloride, CCl_4, was chosen on the basis of compatibility with chlorine, no significant blue spectrum absorption for thin fluid films, and a high affinity for taking chlorine into liquid solution. The latter characteristic is essential to define the effect of solubility on gas zone behavior. The solubility of Cl_2 in CCl_4 and R-11 was experimentally measured using an optical absorption technique. Results of these experiments are shown in Figure 3.4.

3.5 Calibration: Optical System

It was experimentally established that the logarithm of optical absorption was not linearly dependent upon gas concentration. Experimental absorption measurements with known concentrations of chlorine in a 1.4 cm diameter cell established the following relationship between gas content in standard cm^3 per cc and $\ln (I_0/I)$ at λ = 3550 Å and $20.8^{\circ}C$.

$$C_g = 0.39815 \ln (I_0/I) + 0.066075 \left(\ln(I_0/I)\right)^2 \quad \ln\left(\frac{I_0}{I}\right) < 1.35 \quad (3-3)$$
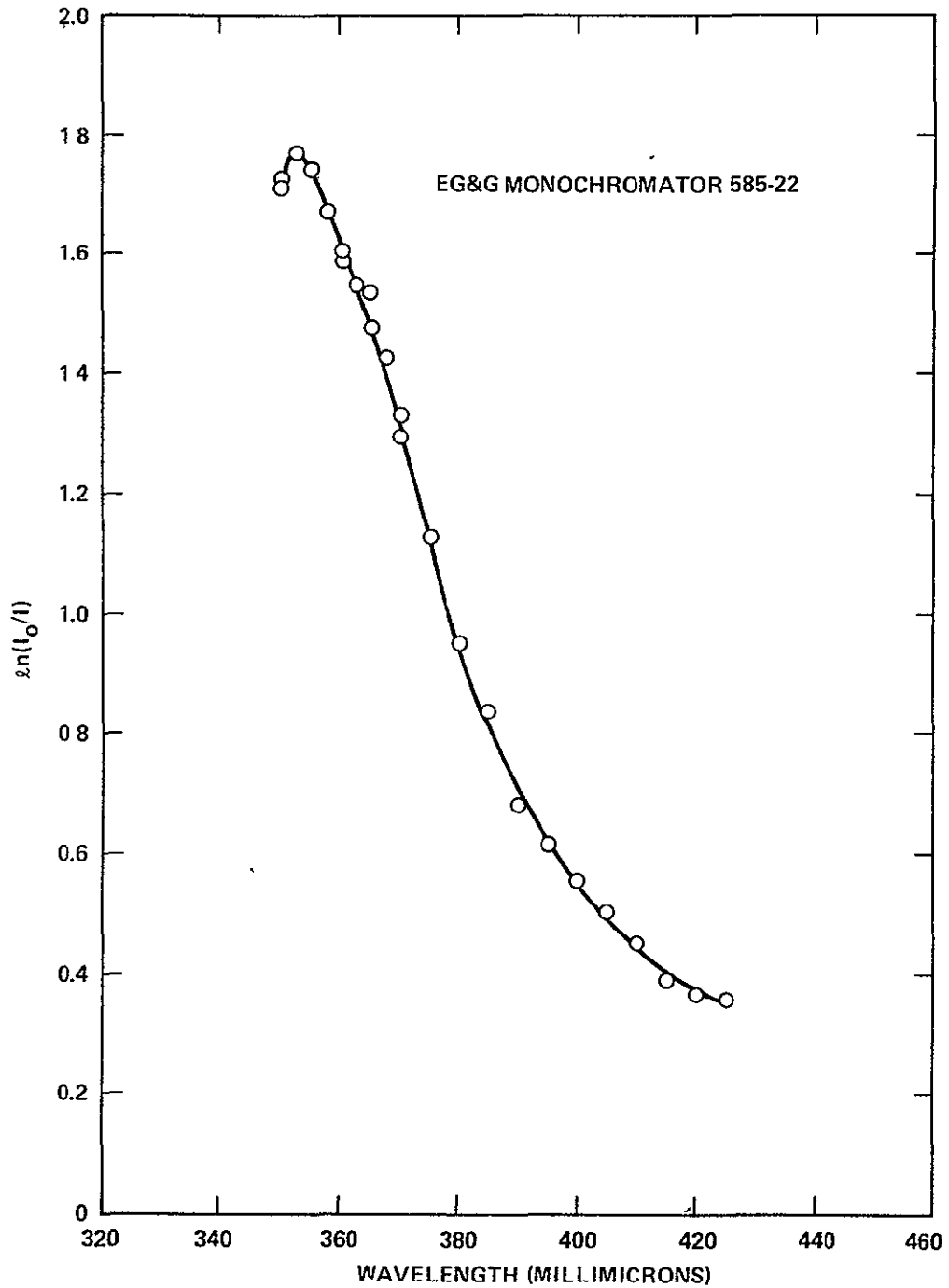
FIGURE 3.3. THE ABSORPTION SPECTRUM OF 1 ATMOSPHERE OF CHLORINE GAS AT 20°C AS A FUNCTION OF WAVELENGTH. AN OPTICAL PATH LENGTH OF APPROXIMATELY 1 CM WAS USED. MONOCHROMATOR BAND-WIDTH WAS NOT DETERMINED.
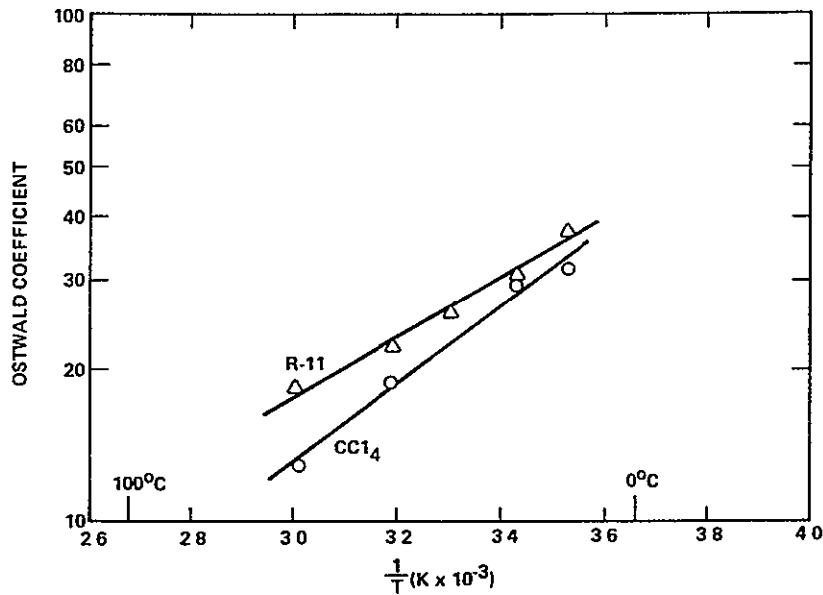
FIGURE 3.4.   THE SOLUBILITY OF CHLORINE IN CCl_4 AND R-11 $(CFCl_3)$

$$C_g = 0.29267 - 0.30541 \, \ell n \, (I_0/I) + 0.49546 \left(\ell n \, (I_0/I)\right)^{1.5}$$

$$\ell n\left(\frac{I_0}{I}\right) \quad 1.35 \qquad (3\text{-}4)$$

The experimental data basis for these expressions is shown in Figure 3.5. At a higher temperature T, the concentration is

$$C_g(T) = 1 - \left[0.0005441 \, \ell n(I_0/I) \, (T\text{-}20.8)\right] \cdot C_g(20.8^\circ C) \qquad (3\text{-}5)$$

The light source employed at all times was a 500-watt slide projector operated from a constant-voltage transformer. The wavelength selected for operation, 3550 Å, was produced with an EG&G monochromator, Model 585-22. Beam thickness at the heat pipe was chosen at 0.1 cm as a compromise between spatial resolution and photodetector resolution. The radiometer detector
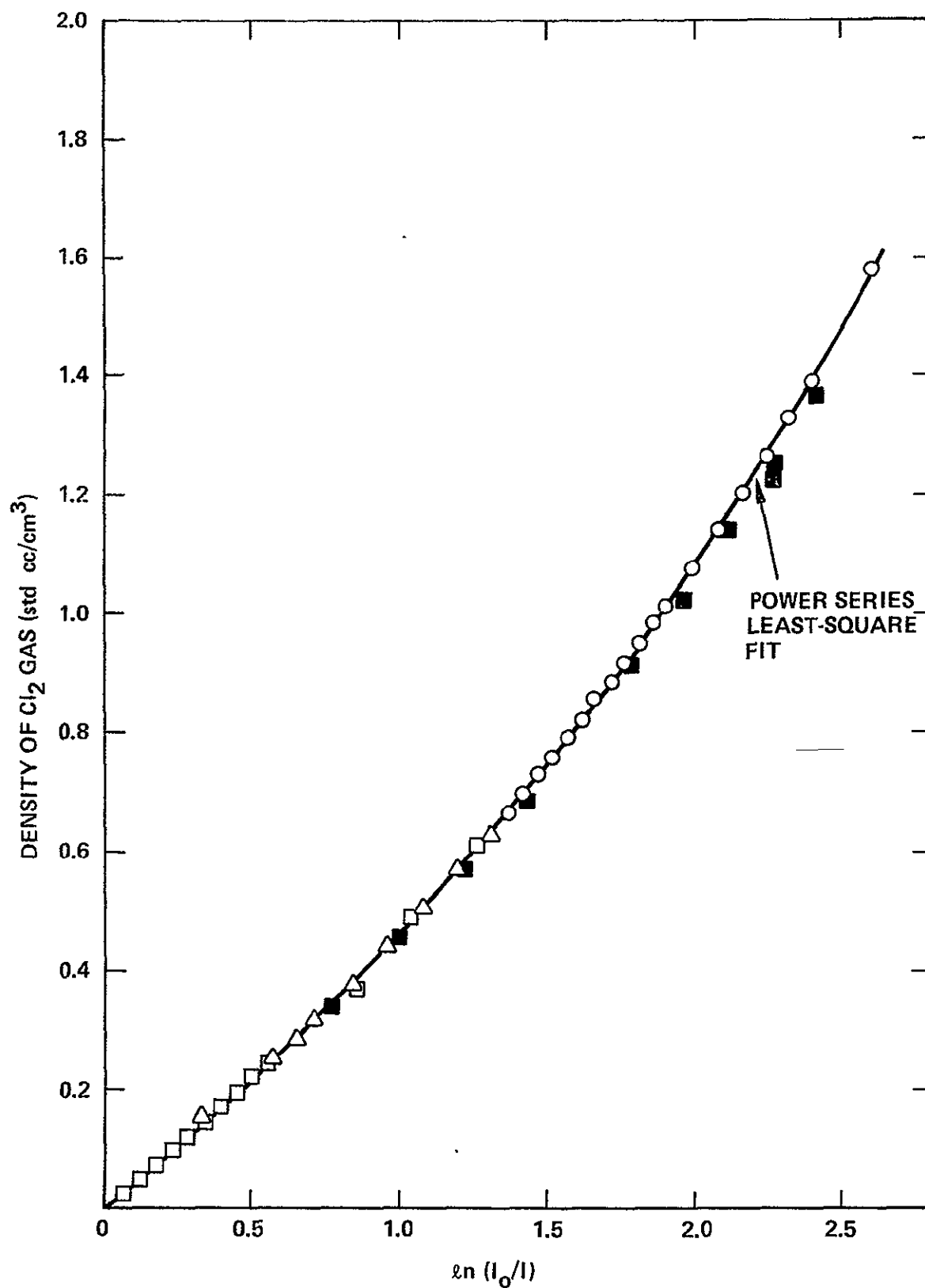
FIGURE 3.5.   EXPERIMENTAL CORRELATION OF GAS CONCENTRATION WITH THE
LOGARITHM OF THE OPTICAL ABSORPTION RATIO FOR A CYLINDRICAL
CELL WITH IDENTICAL PHYSICAL DIMENSIONS TO THE TEST HEAT PIPE.

head and indicator units were also manufactured by EG&G, and were Models
580-22A and 580-11A, respectively.

3.6 Thermal Measurements

Heat sink and heat pipe temperatures were measured using Type K thermo-
couples. Adiabatic temperature was measured with a thermocouple centered in
the adiabatic section on the heat pipe exterior wall. All temperatures were
measured with $0.1^{\circ}C$ resolution using a Doric DS-350 digital thermocouple
indicator.

3.7 Data Reduction

At completion of a test series, data included heat pipe vapor core
temperatures and heat sink temperatures, heat input data, and photometer
current readings as a function of axial position in the heat pipe.

Heat losses or gains through the Dewar surrounding the evaporator and
adiabatic sections were negligible. However, the nylon locator screws at
the condenser entrance form a direct heat leak to the heat sink, and this
heat loss was subtracted from the gross heat input to obtain net heat de-
livered to the condenser. Each set of nylon screws had a combined conduc-
tance of 0.012 W/$^{\circ}$K.

Gas concentrations were calculated using Equations (3-3) through (3-5),
with the sink temperature used as the characteristic temperature in equation
(3-5). The reference photocurrent I_o was based on the peak current immedi-
ately in front of the gas front. For most data runs, this current was about
4.03×10^{-10} ampere. Total gas content within the gas zone was calculated
by numerically integrating the concentration profile with Simpson's Rule.
Gas concentration beyond the farthest measureable condenser position (about
13.7 cm) was assumed equal to the concentration at 13.7 cm.

3.8 Experimental Results

Concentration profiles from experimental sequences using Cl_2/CCl_4 at sink temperatures of $14^\circ C$ and $40^\circ C$ are shown in Figures 3.6 and 3.7, respectively. The axial position scale is with reference to the condenser end nearest the evaporator; e.g., the blind end of the condenser is displaced 16 cm axially from the "front end" of the condenser. The continuous curves, which represent theoretical predictions, are discussed in Section 4. The raw and converted data are both given in complete tabular form in Appendix A.

Vapor temperature response to heat input is displayed in Figure 3.8 for both sink temperatures. Figure 3.9 presents the gas zone molar charge based on integration of the experimental concentration profiles in Figures 3.6 and 3.7. The molar gas load is shown versus stagnant zone gas concentration to determine if gas is going into solution in the stagnant zone. Figure 3.10 presents two models for predicting noncondensable concentration distributions compared with data for the 2.2 W high temperature CCl_4 run.

Analysis of the data presented here is discussed in the following section, Data Interpretation.
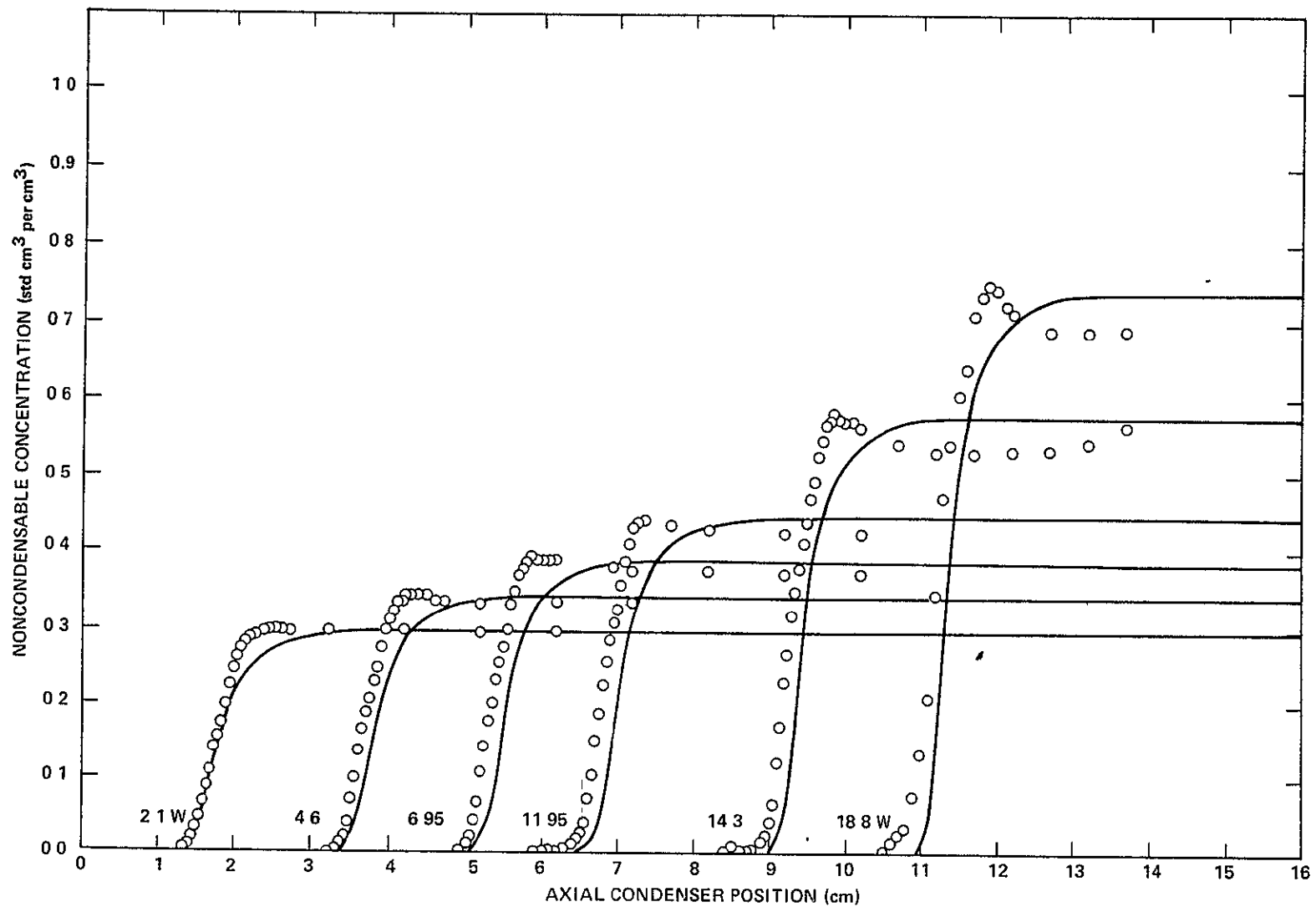
FIGURE 3.6.   A COMPARISON OF EXPERIMENTAL CONCENTRATION PROFILES WITH THE THEORETICAL ONE-DIMENSIONAL MODEL ASSUMING NO SOLUBILITY EFFECTS. GAS CONCENTRATION PROFILES WERE CALCULATED FROM OPTICAL ABSORPTION DATA. SINK TEMPERATURE = 14.°C
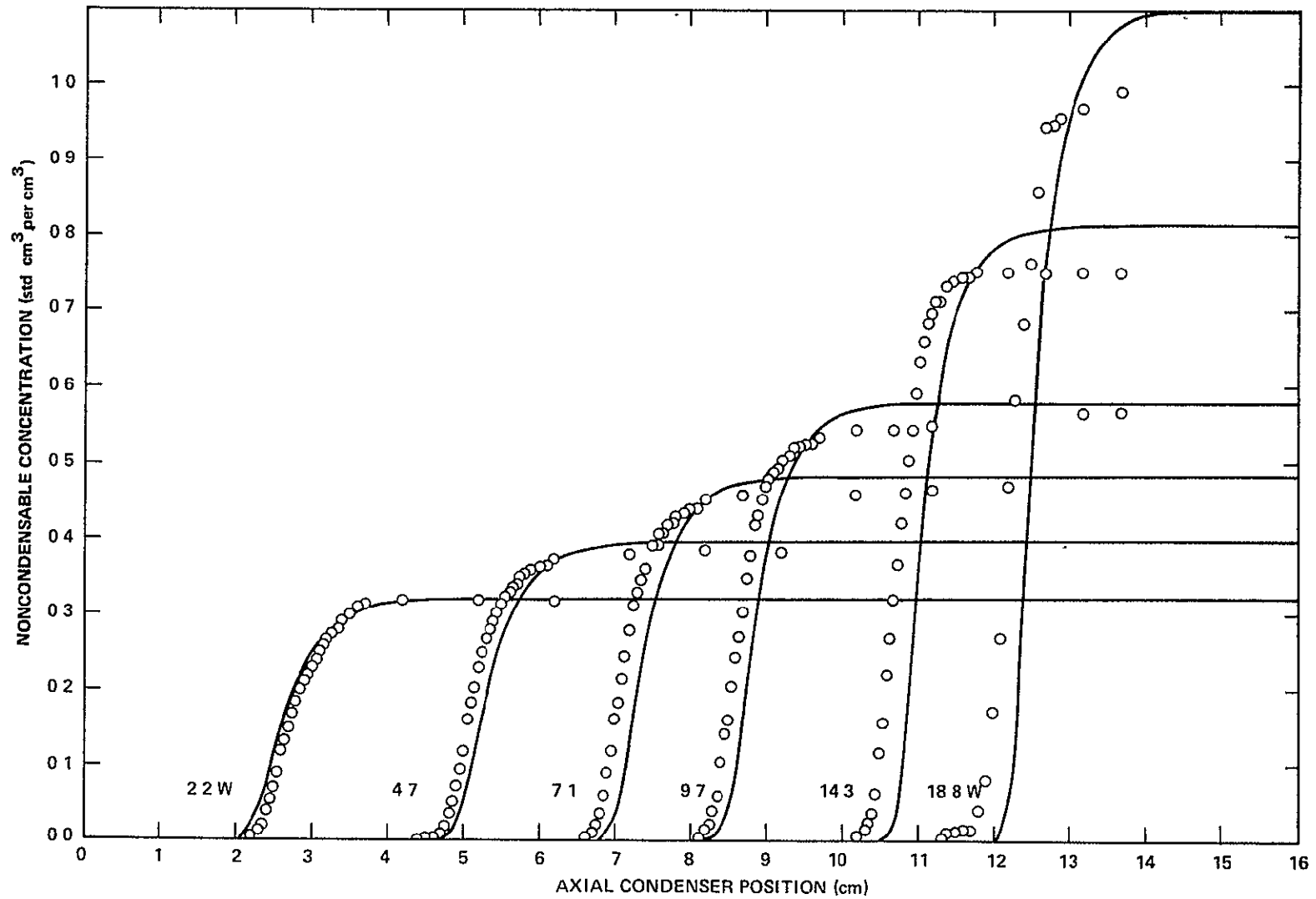
FIGURE 3 7   A COMPARISON OF EXPERIMENTAL CONCENTRATION PROFILES WITH THE THEORETICAL ONE-
DIMENSIONAL MODEL ASSUMING NO SOLUBILITY EFFECTS. GAS CONCENTRATION PROFILES WERE
CALCULATED FROM OPTICAL ABSORPTION DATA   SINK TEMPERATURE = 40.°C
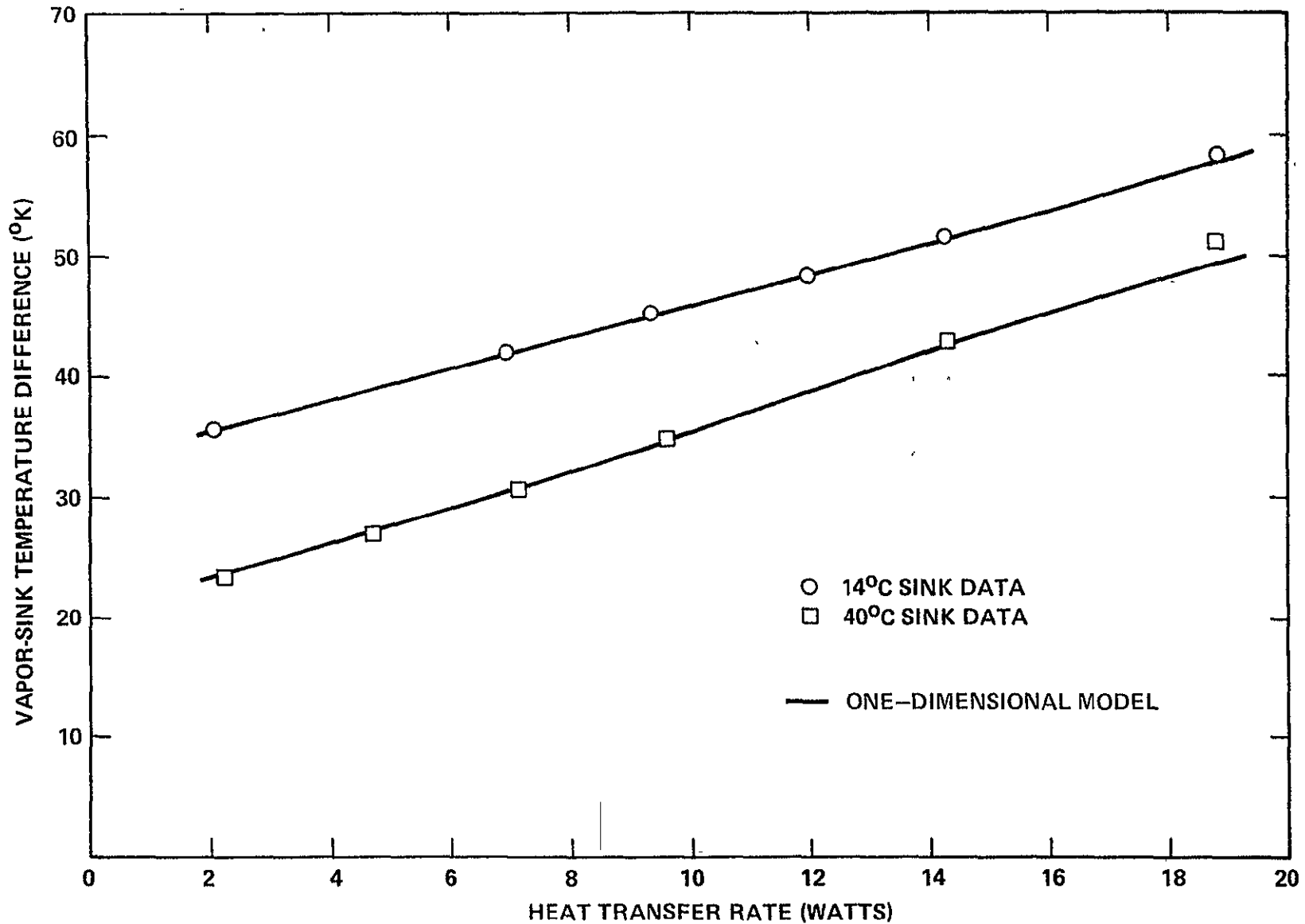
FIGURE 3.8. A COMPARISON OF CALCULATED TEMPERATURE-HEAT TRANSFER CHARACTERISTICS WITH EXPERIMENTAL DATA   CALCULATED VALUES ARE BASED ON THE KNOWN VAPOR-SINK TEMPERATURE DIFFERENCE AND THE NUMERICALLY INTEGRATED TOTAL GAS CONTENT. THIS INFORMATION IS INPUT TO THE ONE-DIMENSIONAL CONDENSATION HEAT TRANSFER MODEL DESCRIBED IN ANALYSIS SECTIONS, AND A GAS PROFILE AND HEAT TRANSFER RATE ARE THEN CALCULATED.
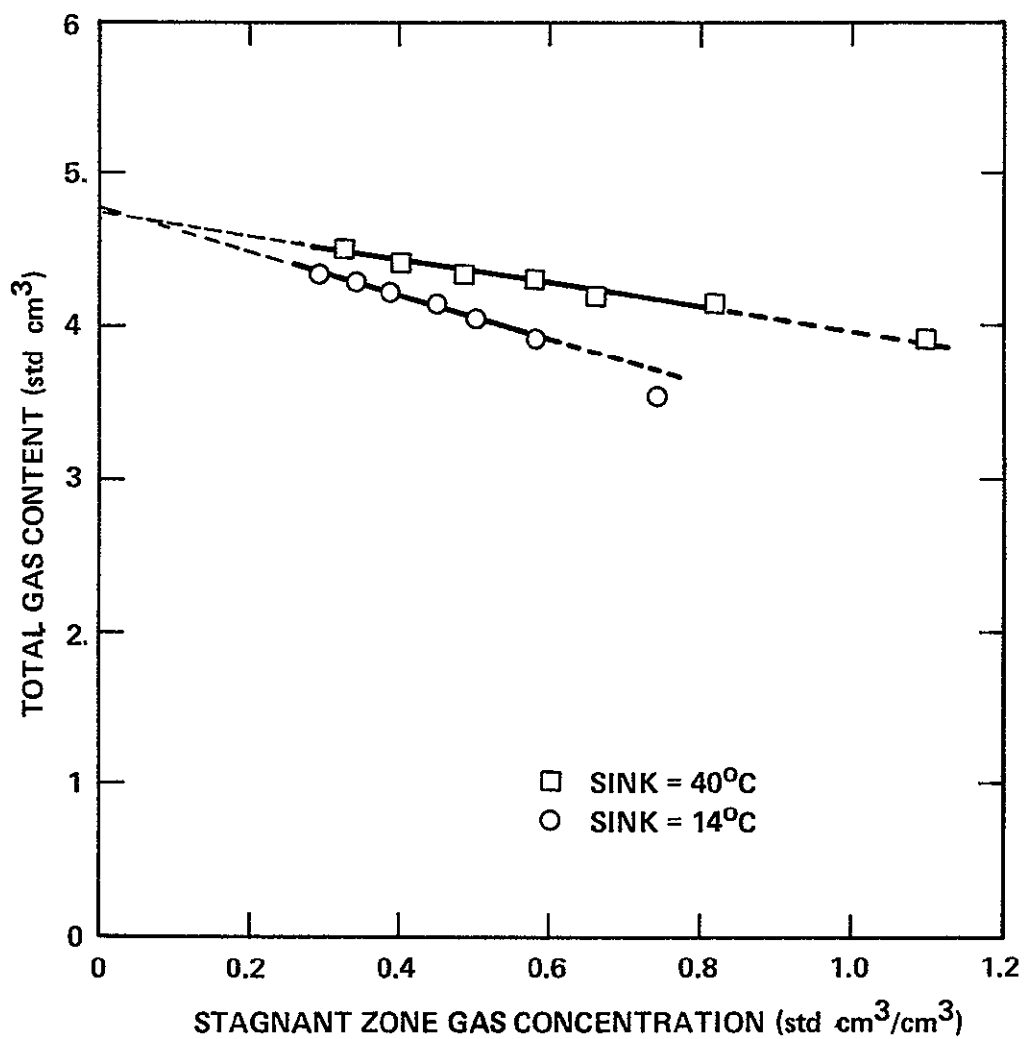
FIGURE 3 9   TOTAL AMOUNT OF NONCONDENSABLE GAS CONTAINED WITHIN STAGNANT GAS
ZONE AS A FUNCTION OF STAGNANT ZONE GAS CONCENTRATION. GAS CONTENT
OBTAINED BY NUMERICALLY INTEGRATING EXPERIMENTALLY-DETERMINED
CONCENTRATION PROFILES. NOTE THAT THE VAPOR PHASE APPEARS TO LOSE
CHLORINE GAS AS THE GAS CONCENTRATION INCREASES.
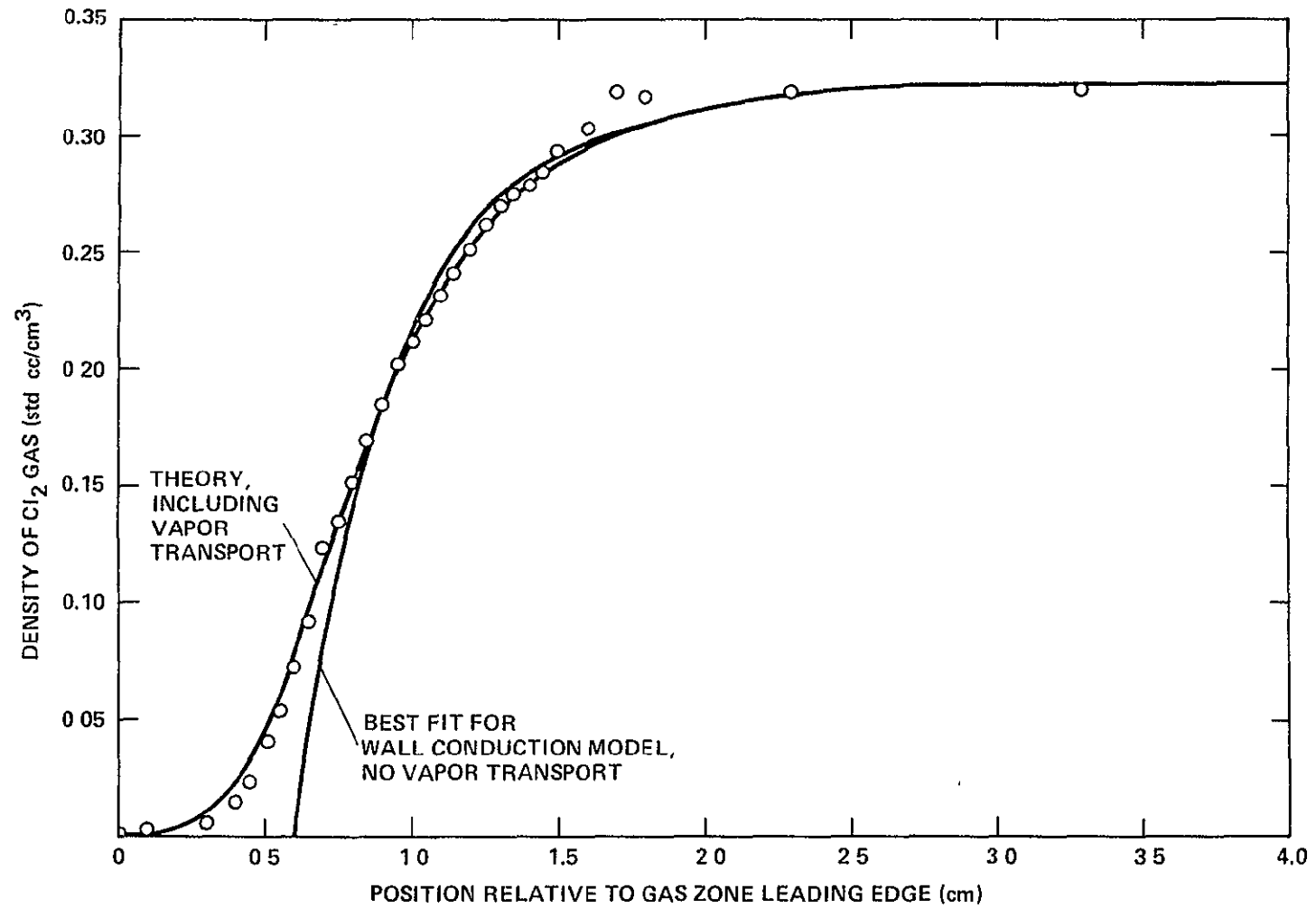
FIGURE 3 10   TWO MODELS FOR PREDICTING NONCONDENSABLE CONCENTRATION DISTRIBUTIONS COMPARED WITH DATA FOR THE 2 2W HIGH TEMPERATURE CCl_4 RUN (SINK = 40°C)   BY MODELING VAPOR DIFFUSION AT THE LEADING EDGE OF THE STAGNANT GAS ZONE, MUCH BETTER AGREEMENT WITH EXPERIMENTAL DATA RESULTS NO SOLUBILITY EFFECTS ARE APPARENT

4.0 DATA INTERPRETATION

4.1 Comparison of Experimental Results With Theory

The full complement of data profiles was simulated with the one-dimensional insoluble gas model and the results are shown in Figures 3.6 and 3.7 as the solid curves. The experimental runs were simulated on the basis of the following data.

1. The vapor-sink driving temperature difference

2. The numerically-integrated experimental total gas content

3. Physical property data and conductances.

With these input data and the governing differential equations, the gas concentration profiles were calculated and the gas front positions determined. The analytical and experimental data are in good general agreement, but the model rather consistently predicts a somewhat shorter gas zone.

The general underestimation of gas zone length by the analytical model is not attributable to the governing differential equations but rather to a discrepancy between the optical absorption-derived gas density in the stagnant zone and the value calculated from the ideal gas law. This difference is summarized in Table 4.1, a comparison of heat transfer and gas concentration data with theory. Although the difference in concentration amounts on the average to only about 5%, it is the cause of the gas front shift. The heat transfer rate as a function of driving temperature difference, given in Figure 3.8 and Table 4.1, is also in agreement to within ±5%; again, the differences are primarily attributable to the discrepancy in gas zone length.

In the low heat flux runs the optically-derived stagnant zone concentrations are in better agreement with the ideal gas law, and the data can be compared with the model in greater detail, as in Figure 3.10. If axial vapor

TABLE 4.1. A COMPARISON OF EXPERIMENTALLY-DETERMINED VALUES
FOR HEAT TRANSFER AND GAS CONCENTRATION WITH VALUES
PREDICTED BY THE ONE-DIMENSIONAL ANALYTICAL MODEL

Sink Temperature (°C)	Vapor-sink Temperature Difference (°C)	Heat Transfer Rate (W)			Stagnant Zone Gas Concentration (std cm^3/cm^3)		
		Expt	Model	% Dev	Expt	Model	% Dev
14 nom.	35.65	2.09	2.05	-1.9	.285	.293	2.8
	38.8	4.58	4.57	-0.2	.330	.340	3.0
	41.8	6.95	7.00	0.7	.377	.388	2.9
	45.05	9.37	9.54	1.8	.427	.445	4.2
	48.2	11.95	12.03	0.7	.482	.508	5.4
	51.45	14.3	14.56	1.8	.565	.579	2.5
	58.17	18.8	19.24	2.3	.691	.740	7.1
40 nom.	23.23	2.22	2.01	-9.5	.330	.323	-2.1
	26.9	4.67	4.57	-2.1	.394	.398	1.0
	30.8	7.13	7.21	1.1	.474	.485	2.3
	34.75	9.65	9.72	0.7	.567	.582	2.6
	38.65	11.92	12.33	3.4	.660	.690	4.5
	42.85	14.3	14.9	4.2	.754	.817	8.4
	51.1	18.8	20.2	7.4	>.993	1.104	-

transport were completely neglected in the modeling, then the gas concentration would be defined by a fin-type axial temperature profile in the stagnant region. This profile has been superimposed on Figure 3.10 to show the influence of vapor diffusion into the stagnant gas. The concentration data of Figure 3.10 are correlated well by the one-dimensional insoluble gas model. Under most operating conditions, the gas concentration profiles did not show any gross effect of the highly soluble gas.

There was, however, a definite "reduction" in noncondensable gas as the stagnant zone gas concentration increased, i.e., as the heat transfer rate was increased. It is very probable that this was due to gas being absorbed into liquid in the stagnant zone. At a sink temperature of $14^{\circ}C$ the Ostwald coefficient for chlorine in carbon tetrachloride is 31.0, while it is 18.5 at $40^{\circ}C$. Assuming no loss of gas from the gas zone, the total moles of gas, N_0, must remain a constant. For a sharply defined gas zone ℓ_g in length, and for a trapped volume of liquid V_ℓ

$$N_0 = (\ell_g A_v + \alpha V) C_{gvm} \qquad (4-1)$$

But in an optical absorption experiment such as done here, only the gas-phase noncondensable is seen, and this observable amount is

$$C_{gvm} \ell_g A_v = N_0 - (\alpha V_\ell) C_{gvm} \qquad (4-2)$$

Therefore, if V_ℓ stays constant, it can be predicted that the observed moles of gas will appear to linearly decrease with increasing stagnant gas concentration, and that the rate of decrease will be proportional to the Ostwald coefficient. Furthermore, in the limit of C_{gvm} going to zero, all test runs

at different sink temperatures should intersect at $C_{gvm} = 0$ and this will represent the total gas content, N_o.

Measured total contents shown in Figure 3.9 are in agreement with all predictions above. The linear rate at which gas is "lost" at $14^o C$ is about 1.9 times the rate at $40^o C$, and the Ostwald coefficient is about 1.7 times higher at $18^o C$ than $40^o C$. In addition, intersection of the two linear gas profiles in Figure 3.9 occurs very close to zero gas concentration. Therefore, the total molar gas content in the heat pipe is about 4.75 std cm^3.

It is informative to now use (4-2) to calculate the amount of liquid contained as droplets and surface film within the stagnant zone. This calculation indicates a liquid load V_ℓ of only 0.039 cm^3 is sufficient to produce the virtual gas loss shown in Figure 3.9.

This effect was the basis of another study[5] where it was shown that under certain conditions a liquid absorption matrix can be used as a gas reservoir for gas-controlled heat pipes. This technique was shown experimentally to reduce reservoir volume by a factor of more than five compared to standard gas reservoir designs.

The high solubility of chlorine in CCl_4 also produced another unique effect not normally encountered in gas-loaded heat pipes. In the tests at low sink temperature, there was an unusual increase in chlorine concentration in the gas front region. This is shown very well in the 18.8 watt run of Figure 3.6. Because the heat pipe is very nearly a constant-pressure system, this zone must actually be _cooler_ than the heat sink. In the fully stagnant zone, the wall and liquid films are close to sink temperature; a higher concentration of chlorine in an intermediate zone implies a local vapor pressure (and film temperature) that must be below sink temperature. Another related

and unusual manifestation of high power level operation was observed in similar experiments carried out with an R-11 heat pipe and chlorine gas. In this case, droplets continuously formed within the vapor phase and fell through the gas front zone until they impinged on upward-moving vapor. This created a stagnation zone of high droplet density. A time-lapse photograph of this phenomenon is shown in Figure 4.1. The vertical streaks are falling droplets, while the lower diffuse disk is the droplet stagnation zone. This photograph was taken through the optical slit of the test apparatus in Figure 3.2a with strong back lighting. This phenomenon is occurring within a tube of only about 1 cm^2 cross-sectional area.

At the 18.8 watt heat flux for each sink temperature, the gas front was also very unstable with large "temporal" fluctuations in the axial concentration profile. The position of the gas front shifted axially 0.15 to 0.20 cm in an erratic fashion with a time constant on the order of 15 to 45 seconds, and the vapor core temperature also fluctuated about $0.1^{o}C$.

The $14^{o}C$ profile is shown in greater detail in A of Figure 4.2, along with a theoretical profile based on the soluble-gas modeling developed in Section 2.2. The axial positions of the experimental and theoretical profiles have been adjusted so that the profiles overlap. The experimental data range is indicated by the bounds given as dotted lines in A of Figure 4.2, while the theoretical profile is displayed as a solid line. The effects of the high chlorine gas solubility on the previously discussed insoluble gas concentration profiles were very modest, and the differences in profile would be indistinguishable in A of Figure 4.2. This was primarily because of the thin fluid films (on the order of 0.001 cm) associated with the vertical reflux mode.

FIGURE 4.1   A TIME-LAPSE PHOTOGRAPH OF DROPLET FORMATION SEEN
             AT 18 WATTS IN A GLASS HEAT PIPE CHARGED WITH Cl_2 AND
             R-11. THE DROPLETS ARE BEING PHOTOGRAPHED WITH
             STRONG BACKLIGHTING THROUGH THE OPTICAL SLOT
             SHOWN IN FIGURE 3 2a. THE DROPLETS FALL UNTIL RESIS-
             TANCE IS ENCOUNTERED FROM UPWARD-MOVING VAPOR,
             CREATING THE DIFFUSE DISC-SHAPED AREA BELOW THE
             FALLING DROPLET STREAK PATTERNS   ONE-SECOND
             ELAPSED TIME.
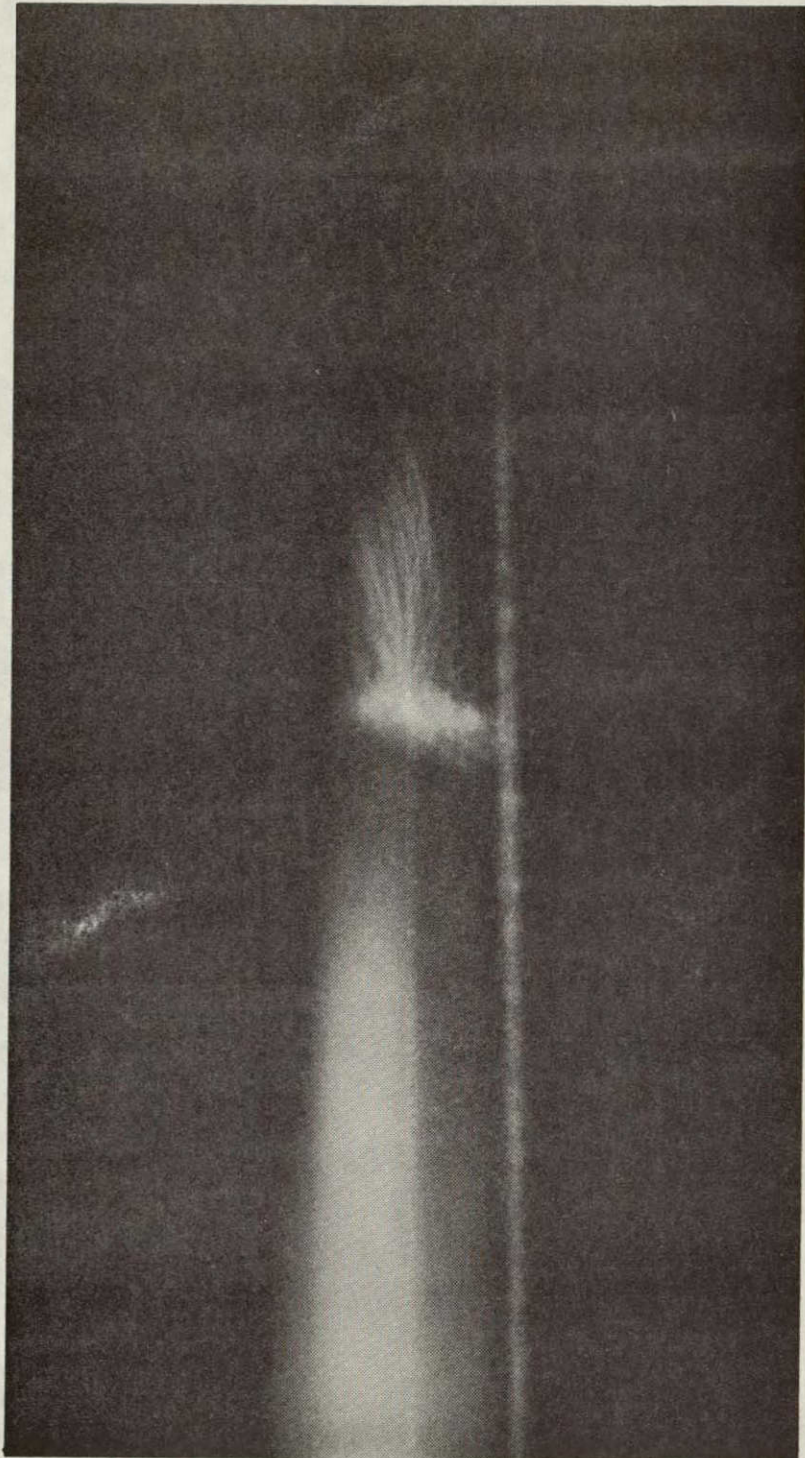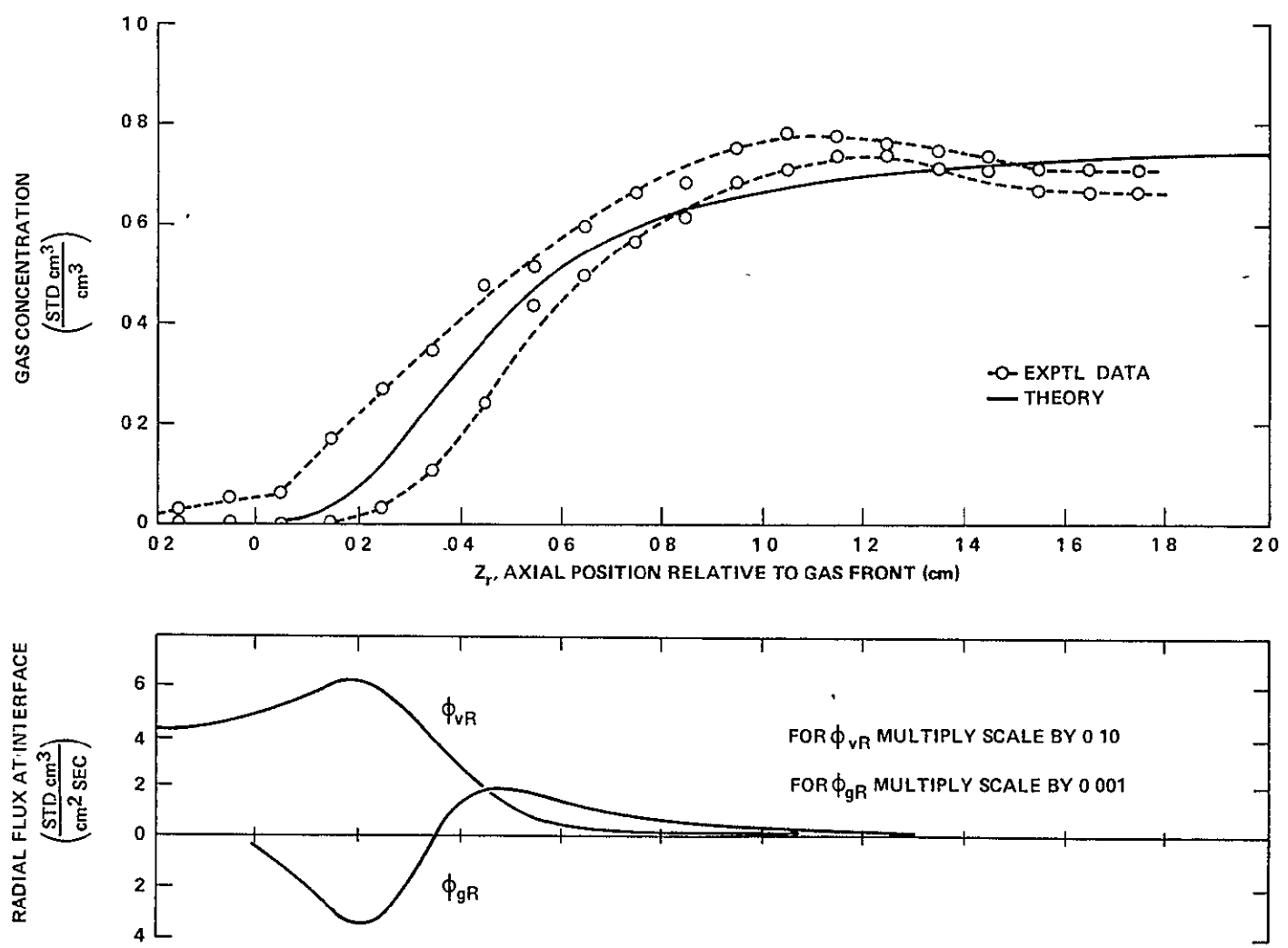
FIGURE 4.2. CONCENTRATION PROFILES AND CALCULATED RADIAL MOLAR FLUX DENSITIES FOR THE 19 WATT, 14°C SINK EXPERIMENTAL RUN. NOTE BAND-STRUCTURE DUE TO FLUCTUATIONS IN GAS CONCENTRATION.

The unsteady gas front behavior is believed to be related to radial free convection. If a Grashof number is calculated based on the tube radius and the vapor-sink temperature difference, a value of about 170,000 is found. For free convection between parallel vertical plates the critical Grashof number is only 8000. If significant radial concentration gradients were present in the transitional zone from free condensation to stagnation, then the radial Grashof number could be high enough to initiate a convective motion, and this unstable convective motion would explain the concentration fluctuations in A of Figure 4.2. This could also explain the cold zone indicated by absorption measurements at the $14^{\circ}C$ sink temperature. A possible scenario leading to this behavior will now be discussed.

In B of Figure 4.2, the calculated radial fluxes of vapor (ϕ_{vR}) and non-condensable gas (ϕ_{gR}) at the liquid-vapor interface are shown. The vapor condensation rate shows a maximum at a point 0.2 cm into the gas zone, and decreases monotonically beyond this point. Chlorine gas is simultaneously being evolved from the film between $0 \leq z_r \leq 0.35$ cm, and dissolved into the film from 0.35 cm to the end of the transition zone. Both the vapor and chlorine radial flux densities are small but finite at 1.05 cm, the position of maximum chlorine concentration in A of Figure 4.2. If the vapor phase gas concentration rises and falls in response to the disordered mass transfer occurring in the first 1/2 cm of the zone, chlorine will be absorbed and desorbed from the liquid film. From Figure 3.4, the heat of solution of Cl_2 in CCl_4 is about 14,000 Joules/g-mole, as calculated from the slope of log α versus 1/T, while the heat of vaporization of CCl_4 is about 31,000 Joules/g-mole in this temperature range. Because the film has 20 to 30 times as much Cl_2 per unit volume as the vapor phase, it is possible that gas desorption from the thin film under semistagnant conditions could lead to a net

cooling of this zone, and a relative maximum in chlorine vapor phase concentration. However, because the modeling and experimental phases of this study were basically one-dimensional approaches, it is not possible to substantiate the mechanisms described above, and these processes should be regarded as speculatory at this time.

4.2 Model Validity

The one-dimensional models developed in this study assume that axial transfer of energy is predominated by diffusive mass transfer and that the sensible heat capacity of the diffusing vapor is negligible compared to the latent heat capacity. These assumptions are validated in Table 4.2, which compares axial transport of heat via gas-phase conduction, ordinary diffusion and thermal diffusion. The comparison was based on the theoretical profile

TABLE 4.2. THE RELATIVE IMPORTANCE OF VARIOUS ENERGY TRANSFER PROCESSES FOR A REPRESENTATIVE CONCENTRATION PROFILE

Mode	Axial Heat Flux Density (W/cm^2)
Conduction	0.0073
Thermal diffusion[1]	0.0004
Latent heat, ordinary diffusion	0.092
Sensible heat, ordinary diffusion[2]	0.015

[1]Assuming a thermal diffusion ratio of 0.05.
[2]Based on the total vapor-sink temperature difference.

in A of Figure 4.2. The comparison was done at the axial position with maximum vapor temperature rate-of-change versus z_r. This position was $z_r = 0.38$ cm. Ordinary diffusion is shown in Table 4.2 to be the primary mode of energy transfer, with heat transfer by conduction accounting for less than 8% of the total thermal flux, and thermal diffusion accounting for less than 0.5% of the energy transfer. The initial assumptions pertaining to energy transport modes are therefore generally satisfied by model solutions. However, the energy associated with vapor phase sensible heat was neglected, yet it could account for up to 15% of the axial energy flux. Inclusion of sensible heat would be an appropriate basis for a more accurate model of gas front concentration profiles.

5.0 SUMMARY

One-dimensional models for condensation in the presence of insoluble and soluble gases have been developed for a tubular geometry. The models have been compared with experimental data derived from Cl_2/CCl_4 vertical reflux heat pipes and are in good agreement with measured concentration profiles at low heat flux densities. At high heat flux densities, the gas fronts become unstable and exhibit a turbulent and fluctuating concentration profile. This turbulent behavior was associated with unusual effects, including an apparent depression of heat pipe wall temperature below sink temperature and the formation of liquid droplets in the vapor phase.

The experimental concentration profiles were determined using a new technique having several advantages over conventional thermocouple or thermistor temperature measurement methods. By selecting a noncondensable gas which strongly absorbs light over discrete portions of the spectrum, the concentration of noncondensable gas as a function of axial position was determined directly from optical absorption measurements in a glass heat pipe. Axial resolution is improved over temperature measuring methods and the vapor-phase flow field is undisturbed.

Apart from the effects at high power level, gas solubility did not have a significant influence on gas concentration profiles. This was predicted by the soluble gas condensation model, and was physically attributable to the relatively thin fluid films (on the order of 0.001 cm) associated with the vertical reflux mode. The short time constants for liquid-phase diffusive equilibrium precluded any significant effect on gas front shape. This may not be true for systems with thicker fluid films or lower liquid phase diffusivities, and each case must be considered individually.

Liquid films and droplets within the stagnant portion of the gas-rich zone were found to create a virtual sink for noncondensable gas. That is, as vapor phase gas concentration was increased, the absorption of increasing amounts of gas within this liquid was detected as a 10 to 20% loss in total moles of noncondensable gas in the vapor phase. This phenomenon could be used in gas-controlled heat pipes to increase thermal control capability or reduce gas reservoir size by dissolving the noncondensable gas into a volumetrically efficient liquid reservoir in lieu of the common gas-bulb reservoir.

REFERENCES

1. B. D. Marcus, _Theory and Design of Variable Conductance Heat Pipes_, NASA Report CR-2018 (April 1972).

2. E. W. Saaski, _Investigation of Arterial Gas Occlusions_, NASA Report CR-114,731 (March 1974).

3. W. F. Ames, _Numerical Methods for Partial Differential Equations_, Barnes and Noble, Inc., New York, 1969.

4. D. Somogyi and H. Yen, _An Approximate Analysis of the Diffusing Flow in a Self-controlled Heat Pipe_, ASME paper 72-HT-M, 1972.

5. E. W. Saaski, _Heat Pipe Temperature Control Utilizing a Soluble Gas Absorption Reservoir_, NASA Contract Report CR 137,792.

APPENDIX A

COMPREHENSIVE TABULATION OF OPTICAL
ABSORPTION AND THERMAL DATA

Run A1

Vapor core temperature:	$49.65^{o}C$
Sink temperature:	$19.2^{o}C$
Heat input:	2.087 W
Calculated gas content:	4.342 std cm^3
Zero-absorption current:	$4.03(\times 10^{-10})$ A

Axial position (cm)	Current $(\times 10^{-10})$A	Concentration (std cm^3/cm^3)
1.294	3.960	.0070
1.344	3.940	.0091
1.394	3.830	.0205
1.444	3.730	.0313
1.494	3.580	.0482
1.544	3.420	.0674
1.594	3.260	.0878
1.644	3.100	.1095
1.694	2.920	.1358
1.744	2.810	.1529
1.794	2.690	.1727
1.844	2.550	.1972
1.894	2.410	.2235
1.944	2.310	.2436
1.994	2.240	.2583
2.044	2.185	.2703
2.094	2.150	.2781
2.144	2.130	.2827
2.194	2.120	.2850
2.244	2.110	.2873
2.294	2.110	.2873
2.344	2.090	.2920
2.394	2.075	.2955
2.494	2.080	.2943
2.594	2.080	.2943
2.694	2.090	.2920
3.194	2.080	.2943
4.194	2.080	.2943
5.194	2.090	.2920
6.194	2.090	.2920
7.194	2.090	.2920
8.194	2.120	.2850
9.194	2.120	.2850
10.194	2.120	.2850
11.194	2.120	.2850
12.194	2.130	.2827
13.194	2.120	.2850

Run A2

Vapor core temperature:	$52.8^{o}C$
Sink temperature:	$14^{o}C$
Heat input:	4.584 W
Calculated gas content:	4.299 std cm^{3}
Zero-absorption current:	$4.03(x\ 10^{-10})$ A

Axial position (cm)	Current $(x\ 10^{-10})$A·	Concentration (std cm^{3}/cm^{3})
1.694	4.080	-.0049
2.194	4.080	-.0049
2.694	4.070	-.0039
2.944	4.070	-.0039
3.094	4.030	.0000
3.194	4.020	.0010
3.294	3.970	.0060 ·
3.344	3.890	.0142
3.394	3.780	.0259
3.444	3.630	.0425
3.494	3.390	.0711
3.544	3.170	.0998
3.594	2.910	.1373
3.644	2.740	.1643
3.694	2.610	.1865
3.744	2.510	.2045
3.794	2.380	.2294
3.844	2.300	.2457
3.894	2.180	.2714
3.944	2.080	.2943
3.994	2.020	.3088
4.044	1.970	.3212
4.094	1.930	.3315
4.144	1.925	.3328
4.194	1.890	.3420
4.244	1.890	.3420
4.294	1.890	.3420
4.344	1.890	.3420
4.394	1.890	.3420
4.494	1.890	.3420
4.594	1.930	.3315
4.694	1.930	.3315
5.194	1.940	.3289
6.194	1.930	.3315
7.194	1.930	.3315
8.194	1.940	.3289
9.194	1.940	.3289
10.194	1.940	.3289
11.194	1.940	.3289
12.194	1.940	.3289
13.194	1.935	.3302

Run A3

Vapor core temperature:	$55.8^{\circ}C$
Sink temperature:	$14.05^{\circ}C$
Heat input:	6.949 W
Calculated gas content:	4.22 std cm^3
Zero-absorption current:	4.03 (x 10^{-10}) A

Axial position (cm)	Current (x 10^{-10})A	Concentration (std cm^3/cm^3)
1.694	4.080	-.0049
2.194	4.080	-.0049
2.694	4.060	-.0030
3.194	4.040	-.0010
3.694	3.940	.0091
4.194	4.020	.0010
4.694	4.030	.0000
4.794	4.030	.0000
4.894	3.990	.0040
4.994	3.910	.0121
5.044	3.820	.0216
5.094	3.630	.0425
5.144	3.430	.0662
5.194	3.120	.1067
5.244	2.880	.1419
5.294	2.680	.1744
5.344	2.540	.1990
5.394	2.380	.2294
5.444	2.270	.2519
5.494	2.170	.2736
5.544	2.065	.2979
5.594	1.940	.3289
5.644	1.870	.3474
5.694	1.800	.3668
5.744	1.780	.3725
5.794	1.740	.3842
5.844	1.710	.3932
5.894	1.730	.3872
5.944	1.730	.3872
5.994	1.730	.3872
6.094	1.730	.3872
6.194	1.730	.3872
6.694	1.760	.3783
7.194	1.780	.3725
8.194	1.780	.3725
9.194	1.790	.3696
10.194	1.780	.3725
11.194	1.780	.3725
12.194	1.790	.3696
13.194	1.764	.3771

Run A4

Vapor core temperature:	$59^{o}C$
Sink temperature:	$13.95^{o}C$
Heat input:	9.369 W
Calculated gas content:	4.142 std cm^3
Zero-absorption current:	4.02(x 10^{-10}) A

Axial position (cm)	Current (x 10^{-10})A	Concentration (std cm^3/cm^3)
2.194	4.080	-.0059
3.194	4.020	.0000
4.194	3.970	.0050
5.194	3.980	.0040
5.694	3.990	.0030
5.794	3.940	.0081
5.894	3.990	.0030
5.994	3.990	.0030
6.094	3.980	.0040
6.194	3.970	.0050
6.294	3.940	.0081
6.394	3.900	.0122
6.444	3.830	.0195
6.494	3.770	.0259
6.544	3.640	.0403
6.594	3.370	.0726
6.644	3.130	.1042
6.694	2.820	.1502
6.744	2.610	.1853
6.794	2.410	.2224
6.844	2.260	.2529
6.894	2.120	.2838
6.944	2.030	.3051
6.994	1.890	.3408
7.044	1.835	.3557
7.094	1.730	.3859
7.144	1.650	.4105
7.194	1.590	.4300
7.244	1.570	.4367
7.294	1.560	.4401
7.344	1.560	.4401
7.394	1.560	.4401
7.694	1.580	.4334
8.194	1.600	.4267
9.194	1.610	.4234
10.194	1.610	.4234
11.194	1.610	.4234
12.194	1.610	.4234
13.194	1.600	.4267

Run A5

Vapor core temperature:	62.3°C	
Sink temperature:	14.1°C	
Heat input:	11.952 W	
Calculated gas content:	4.046 std cm^3	
Zero-absorption current:	4.04($\times 10^{-10}$) A	

Axial position (cm)	Current ($\times 10^{-10}$)A	Concentration (std cm^3/cm^3)
2.194	4.120	-.0078
3.194	4.040	.0000
4.194	3.980	.0060
5.194	3.960	.0080
6.194	3.930	.0111
7.194	3.980	.0060
7.494	3.990	.0050
7.594	3.980	.0060
7.694	3.940	.0101
7.794	3.780	.0269
7.844	3.640	.0424
7.894	3.370	.0747
7.944	3.090	.1120
7.994	2.760	.1621
8.044	2.475	.2122
8.094	2.275	.2521
8.144	2.120	.2862
8.294	1.980	.3199
8.244	1.873	.3478
8.294	1.780	.3738
8.344	1.680	.4037
8.394	1.590	.4326
8.444	1.500	.4637
8.494	1.425	.4915
8.544	1.410	.4972
8.594	1.376	.5106
8.644	1.367	.5142
8.694	1.370	.5130
8.794	1.370	.5130
8.894	1.400	.5011
8.994	1.405	.4992
9.094	1.406	.4988
9.194	1.415	.4953
10.194	1.480	.4709
11.194	1.450	.4820
12.194	1.450	.4820

Run A6

Vapor core temperature:	$65.65^{o}C$
Sink temperature:	$14.2^{o}C$
Heat input:	14.263 W
Calculated gas content:	3.92 std cm^3
Zero-absorption current:	$3.98(x\ 10^{-10})$ A

Axial position (cm)	Current (x 10^{-10})A	Concentration (std cm^3/cm^3)
2.194	3.830	.0154
3.194	3.820	.0165
4.194	3.840	.0144
5.194	3.920	.0061
6.194	3.940	.0040
7.194	3.980	.0000
8.194	3.970	.0010
8.394	3.940	.0040
8.494	3.880	.0102
8.594	3.920	.0061
8.694	3.930	.0051
8.794	3.930	.0051
8.894	3.850	.0133
8.944	3.730	.0262
8.994	3.580	.0431
9.044	3.380	.0671
9.094	2.980	.1213
9.144	2.680	.1687
9.194	2.360	.2275
9.244	2.180	.2654
9.294	1.970	.3150
9.344	1.844	.3481
9.394	1.740	.3778
9.444	1.630	.4117
9.494	1.550	.4382
9.544	1.460	.4702
9.594	1.400	.4930
9.644	1.320	.5253
9.694	1.270	.5468
9.744	1.220	.5694
9.794	1.210	.5741
9.844	1.185	.5859
9.894	1.210	.5741
9.944	1.210	.5741
9.994	1.215	.5717
10.094	1.215	.5717
10.194	1.230	.5648
10.694	1.280	.5424
11.194	1.305	.5317
11.694	1.120	.5295
12.194	1.300	.5338
12.694	1.300	.5338
13.194	1.276	.5442
13.694	1.230	.5648

Run A7

Vapor core temperature:	$72.27^{\circ}C$
Sink temperature:	$14.1^{\circ}C$
Heat input:	18.802 W
Calculated gas content:	3.534 std cm^3
Zero-absorption current:	$4.03(\times 10^{-10})$ A

Axial position (cm)	Current $(\times 10^{-10})A$	Concentration (std cm^3/cm^3)
2.194	4.300	-.0256
3.194	4.100	-.0069
4.194	4.000	.0030
5.194	3.900	.0132
6.194	3.850	.0184
7.194	3.820	.0216
8.194	3.600	.0459
9.194	4.020	.0010
10.194	3.980	.0050
10.294	3.980	.0050
10.394	4.030	.0000
10.494	4.000	.0030
10.594	3.880	.0152
10.694	3.780	.0259
10.794	3.750	.0291
10.894	3.350	.0761
10.994	2.950	.1313
11.094	2.500	.2064
11.194	1.890	.3420
11.294	1.480	.4696
11.394	1.300	.5407
11.494	1.160	.6052
11.594	1.090	.6413
11.694	.965	.7121
11.794	.926	.7371
11.894	.907	.7499
11.994	.916	.7438
12.094	.945	.7247
12.194	.960	.7152
12.694	1.000	.6910
13.194	1.000	.6910
13.694	1.000	.6910

Run B1

Vapor core temperature:	$63.35^{o}C$
Sink temperature:	$40.12^{o}C$
Heat input:	2.221 W
Calculated gas content:	4.498 std cm^3
Zero-absorption current:	$4.03(\times 10^{-10})$ A

Axial position (cm)	Current ($\times 10^{-10}$)A	Concentration (std cm^3/cm^3)
1.294	3.920	.0111
1.694	4.000	.0030
1.794	4.030	.0000
1.894	4.030	.0000
1.994	4.010	.0020
2.094	4.020	.0010
2.194	3.980	.0050
2.294	3.890	.0142
2.344	3.810	.0227
2.394	3.660	.0392
2.444	3.540	.0530
2.494	3.380	.0724
2.544	3.230	.0918
2.594	3.030	.1195
2.644	2.925	.1350
2.694	2.820	.1512
2.744	2.705	.1699
2.794	2.620	.1844
2.844	2.520	.2022
2.894	2.470	.2115
2.944	2.420	.2210
2.994	2.370	.2307
3.044	2.320	.2408
3.094	2.270	.2511
3.144	2.220	.2617
3.194	2.180	.2704
3.244	2.165	.2737
3.294	2.140	.2793
3.344	2.120	.2838
3.394	2.080	.2930
3.494	2.035	.3037
3.594	1.970	.3196
3.694	1.980	.3171
4.194	1.970	.3196
5.194	1.970	.3196
6.194	1.970	.3196
7.194	1.970	.3196
8.194	1.940	.3272
9.194	1.960	.3221
10.194	1.970	.3196
11.194	1.970	.3196
12.194	1.990	.3146
13.194	1.940	.3272
13.694	1.930	.3297

Run B2

Vapor core temperature: 57.1°C

Sink temperature: 40.2°C

Heat input: 4.667 W

Calculated gas content: 4.421 std cm^3

Zero-absorption current: 4.03(x10^{-10}) A

Axial position (cm)	Current (x 10^{-10})A$^-$	Concentration (std cm^3/cm^3)
1.694	4.030	.0000
2.194	4.060	-.0030
2.694	4.060	-.0030
3.194	4.060	-.0030
3.694	3.970	.0060
4.194	4.020	.0010
4.294	4.020	.0010
4.394	4.010	.0020
4.494	3.990	.0040
4.594	3.980	.0050
4.694	3.910	.0121
4.744	3.820	.0216
4.794	3.680	.0368
4.844	3.530	.0540
4.894	3.360	.0747
4.944	3.180	.0981
4.944	3.020	.1204
5.044	2.740	.1634
5.094	2.610	.1853
5.144	2.500	.2050
5.194	2.355	.2326
5.244	2.265	.2509
5.294	2.180	.2690
5.344	2.120	.2824
5.394	2.070	.2939
5.444	2.025	.3045
5.494	1.980	.3155
5.544	1.940	.3254
5.594	1.930	.3280
5.644	1.890	.3383
5.694	1.880	.3409
5.744	1.840	.3516
5.794	1.820	.3570
5.894	1.800	.3626
5.994	1.790	.3654
6.094	1.780	.3682
6.194	1.753	.3759
7.194	1.730	.3825
8.194	1.720	.3854
9.194	1.730	.3825
10.194	1.710	.3884
11.194	1.710	.3884
12.194	1.730	.3825
13.194	1.700	.3914
13.694	1.690	.3944

Run B3

Vapor core temperature:	70.95^{o}C
Sink temperature:	40.15^{o}C
Heat input:	7.13 W
Calculated gas content:	4.337 std cm^3
Zero-absorption current:	4.03($\times 10^{-10}$) A

Axial position (cm)	Current ($\times 10^{-10}$)A	Concentration (std cm^3/cm^3)
2.194	4.030	.0000
3.194	4.030	.0000
4.194	3.990	.0040
5.194	4.020	.0020
6.194	4.010	.0020
6.294	4.010	.0020
6.394	4.010	.0020
6.494	4.020	.0010
6.594	3.980	.0050
6.694	3.910	.0121
6.744	3.810	.0226
6.794	3.670	.0379
6.844	3.480	.0599
6.894	3.230	.0914
6.944	3.020	.1204
6.994	2.750	.1618
7.044	2.620	.1836
7.094	2.440	.2162
7.144	2.285	.2468
7.194	2.120	.2824
7.244	1.990	.3130
7.294	1.920	.3305
7.344	1.855	.3476
7.394	1.800	.3626
7.444	1.660	.4035
7.494	1.700	.3914
7.544	1.690	.3944
7.594	1.650	.4066
7.644	1.640	.4097
7.694	1.605	.4208
7.744	1.600	.4224
7.794	1.570	.4322
7.844	1.560	.4355
7.894	1.560	.4355
7.994	1.540	.4422
8.094	1.540	.4422
8.194	1.505	.4541
8.694	1.490	.4594
10.194	1.490	.4594
11.194	1.470	.4665
12.194	1.480	.4629
13.194	1.470	.4665
13.694	1.450	.4737

Run B4

Vapor core temperature:	74.85^o
Sink temperature:	40.1^o
Heat input:	9.653 W
Calculated gas content:	4.309 std cm^3
Zero-absorption current:	4.03(x 10^{-10}) A

Axial position (cm)	Current (x 10^{-10})A	Concentration (std cm^3/cm^3)
2.194	4.030	.0000
3.194	4.030	.0000
4.194	3.980	.0050
5.194	4.010	.0020
6.194	3.990	.0040
7.194	4.020	.0010
7.694	4.020	.0010
7.794	4.000	.0030
7.894	3.990	.0040
7.994	3.990	.0040
8.094	3.980	.0050
8.194	3.870	.0163
8.244	3.820	.0216
8.294	3.630	.0424
8.344	3.400	.0697
8.394	3.140	.1036
8.444	2.870	.1428
8.494	2.750	.1618
8.544	2.490	.2068
8.594	2.295	.2447
8.644	2.165	.2723
8.694	2.020	.3057
8.744	1.845	.3503
8.794	1.740	.3796
8.844	1.160	.4192
8.894	1.560	.4355
8.944	1.150	.4524
8.994	1.460	.4701
9.044	1.425	.4829
9.094	1.405	.4904
9.144	1.395	.4942
9.194	1.370	.5038
9.244	1.360	.5078
9.294	1.350	.5117
9.344	1.320	.5238
9.394	1.320	.5238
9.494	1.310	.5279
9.594	1/310	.5279
9.694	1.290	.5362
10.194	1.270	.5447
10.694	1.270	.5447
11.194	1.260	.5490
12.194	1.230	.5622
13.194	1.220	.5667
13.694	1.220	.5667

Run B5

Vapor core temperature:	$78.87^\circ C$
Sink temperature:	$40.22^\circ C$
Heat input:	11.916 W
Calculated gas content:	4.195 std cm^3
Zero-absorption current:	4.03(x 10^{-10}) A

Axial position (cm)	Current (x 10^{-10})A	Concentration (std cm^3/cm^3)
2.194	4.020	.0010
3.194	4.030	.0000
4.194	3.980	.0050
5.194	4.020	.0010
6.194	4.010	.0020
7.194	4.010	.0020
8.194	3.990	.0040
9.194	4.020	.0010
9.294	3.970	.0060
9.394	3.830	.0205
9.444	3.670	.0379
9.494	3.380	.0722
9.544	3.120	.1063
9.594	2.810	.1522
9.644	2.540	.1977
9.694	2.330	.2376
9.744	2.120	.2824
9.794	1.935	.3267
9.844	1.790	.3654
9.894	1.673	.3995
9.944	1.560	.4354
9.994	1.440	.4773
10.044	1.350	.5117
10.094	1.276	.5421
10.144	1.230	.5622
10.194	1.180	.5850
10.244	1.175	.5874
10.294	1.166	.5916
10.344	1.140	.6042
10.394	1.130	.6091
10.444	1.125	.6116
10.494	1.120	.6141
10.594	1.110	.6191
10.694	1.080	.6345
10.794	1.080	.6345
10.894	1.080	.6345
11.194	1.070	.6398
12.194	1.080	.6345
13.194	1.135	.6066
13.694	1.030	.6607

Run B6

Vapor core temperature:	$83.1^{\circ}C$
Sink temperature:	$40.25^{\circ}C$
Heat input:	14.336 W
Calculated gas content:	4.157 std cm^3
Zero-absorption current:	$4.04(x\ 10^{-10})$ A

Axial position (cm)	Current (x 10^{-10})A	Concentration (std cm^3/cm^3)
2.194	4.040	.0000
3.194	4.030	.0010
4.194	4.030	.0010
5.194	4.030	.0010
6.194	4.020	.0020
7.194	3.980	.0060
8.194	4.000	.0040
9.194	4.040	.0000
9.694	4.030	.0010
9.994	3.990	.0050
10.094	3.980	.0060
10.194	3.980	.0060
10.294	3.890	.0152
10.344	3.830	.0215
10.394	3.690	.0367
10.444	3.470	.0622
10.494	3.050	.1172
10.544	2.780	.1580
10.594	2.420	.2211
10.644	2.180	.2702
10.694	1.970	.3191
10.744	1.790	.3666
10.794	1.605	.4220
10.844	1.490	.4607
10.894	1.370	.5051
10.944	1.270	.5460
10.994	1.165	.5935
11.044	1.080	.6359
11.094	1.030	.6620
11.140	0.980	.6673
11.194	0.965	.6990
11.244	0.936	.7168
11.294	0.938	.7155
11.394	0.908	.7348
11.494	0.895	.7434
11.594	0.890	.7468
11.694	0.890	.7468
11.794	0.880	.7536
12.194	0.880	.7536
12.694	0.880	.7536
13.194	0.880	.7536
13.694	0.880	.7536

Run B7

Vapor core temperature:	$91.3^{\circ}C$
Sink temperature:	$40.2^{\circ}C$
Heat input:	18.807 W
Calculated gas content:	3.915 std cm^3
Zero-absorption current:	$4.03(x\ 10^{-10})$ A

Axial position (cm)	Current (x 10^{-10})A	Concentration (std cm^3/cm^3)
2.194	4.020	.0010
3.194	4.020	.0010
4.194	2.980	.1263
5.194	4.020	.0010
6.194	3.980	.0050
7.194	3.980	.0050
8.194	3.940	.0091
9.194	4.070	-.0039
10.194	4.050	-.0020
10.694	4.030	.0000
11.194	4.030	.0000
11.294	4.000	.0030
11.394	3.900	.0132
11.494	3.900	.0132
11.594	3.880	.0152
11.694	3.870	.0163
11.794	3.640	.0413
11.894	3.300	.0823
11.994	2.680	.1733
12.094	2.180	.2690
12.194	1.460	.4701
12.294	1.180	.5850
12.394	0.985	.6859
12.494	0.860	.7661
12.594	2.741	.8604
12.694	0.650	.9487
12.794	0.650	.9487
12.894	0.640	.9594
13.194	0.630	.9704
13.694	2.610	.9932

APPENDIX B

SELECTED TABULATIONS OF CALCULATED TEMPERATURE AND
CONTENTRATION PROFILES BASED ON THE 1-DIMENSIONAL
INSOLUBLE GAS MODEL

NOTE: The ":" sign appearing in the printout is a misprint for the numeral "3".

Vapor Temperature	$49.65\,^{\circ}C$
Sink Temperature	$14.0\,^{\circ}F$
Gas Content	4.342 std cm^3
Calculated Heat Transfer Rate	20.47 W

Axial Position (cm)	T_W^+	T_V^+	Gas Concentration (std cm3/cm3)
.914829	.923974	1.0	0.0
.94531	.92935		
.97793	.928676		
1.00935	.927843		
1.04076	.926935		
1.07224	.925775		
1.10772	.91426		
1.13521	.922291		
1.16669	.919713		
1.19817	.91632		
1.22965	.911942	.935	.822423E-2
1.26114	.906295	.945303	.341373E-2
1.29262	.894435	.929359	.516373E-2
1.3241	.891011	.992732	.754087E-2
1.45558	.890763	.974326	.110974E-1
1.35707	.86947	.954412	.156224E-1
1.41855	.552917	.950553	.215202E-1
1.45003	.596265	.534323	.256775E-1
1.48151	.817555	.912068	.377375E-1
1.515	.79571	.996962	.480204E-1
1.54448	.771554	.957911	.595605E-1
1.57596	.745325	.825616	.720926E-1
1.60744	.7173	.790602	.352536E-1
1.63893	.697953	.7536	.897394E-1
1.67041	.657377	.715339	.112193
1.70189	.526272	.675721	.125341
1.73337	.534924	.638255	.137960
1.76486	.553694	.600522	.149921
1.79634	.522657	.55396	.161121
1.82782	.502697	.529313	.171532
1.8593	.473403	.495278	.181157
1.89079	.445125	.463429	.190022
1.92227	.41797	.433297	.19917
1.95375	.392007	.404365	.205651
1.98523	.367275	.378095	.212517
2.01672	.343766	.352901	.218919
2.0482	.321535	.329243	.224605
2.07968	.300504	.307032	.22999
2.11117	.28066	.286211	.234505

Run A1 (continued)

2.14265	.251967	.25569	.2393
2.17413	.24428)	.248404	.243435
2.20561	.227857	.241285	.247243
2.2371	.212347	.215267	.250751
2.26858	.197901	.200996	.253924
2.30006	.124172	.186883	.256966
2.33154	.171411	.173193	.259713
2.36303	.15947	.160979	.262257
2.39451	.143305	.149572	.264601
2.42599	.137571	.139929	.266766
2.45747	.123125	.123001	.268767
2.48896	.119057	.113745	.270615
2.52044	.110538	.111118	.272324
2.55192	.10262	.103032	.273903
2.5834	.952388E-1	.955972E-1	.275263
2.61489	.833605E-1	.336975E-1	.276714
2.64637	.819535E-1	.221457E-1	.277962
2.67785	.759281E-1	.761135E-1	.279117
2.70933	.704357E-1	.705046E-1	.280196
2.74082	.652699E-1	.652901E-1	.281174
2.7723	.604654E-1	.604443E-1	.282088
2.80378	.559966E-1	.559427E-1	.282934
2.83526	.518473E-1	.517622E-1	.283716
2.86675	.479909E-1	.478312E-1	.284439
2.89823	.444085E-1	.442794E-1	.285108
2.92971	.041033	.040938	.285727
2.96119	.379966E-1	.378291E-1	.286299
2.99268	.351371E-1	.034966	.286928
3.02416	.324772E-1	.320021E-1	.287317
3.05564	.300142E-1	.299359E-1	.287769
3.08712	.277926E-1	.275505E-1	.289185
3.11861	.256174E-1	.254549E-1	.28857?
3.15009	.235584E-1	.234756E-1	.28?939
3.18157	.213445E-1	.216352E-1	.28985?
3.21306	.201553E-1	.159274E-1	.28957?
3.24454	.15411?E-1	.01542?	.289944
3.27602	.171756E-1	.17003?E-1	.29010?
3.3075	.015844	.15478?E-1	.29024?
3.33899	.146147E-1	.144245E-1	.29054?
3.37047	.134794E-1	.132425E-1	.29073?
3.40195	.124395E-1	.12290?E-1	.290955
3.43343	.114586E-1	.110164E-1	.29112?
3.46492	.105629E-1	.01045?	.29123?
3.4964	.973597E-2	.96054?E-2	.291435
3.52788	.897259E-2	.884934E-2	.29157?
3.55936	.85682E-2	.915151E-2	.291695
3.59085	.751951E-2	.750781E-2	.29121?
3.62233	.701945E-2	.691472E-2	.29191?

Run A1 (continued)

3.65031	.646706E-2	.626525E-2	.292017
3.6852?	.595792E-2	.586465E-2	.292107
3.7157?	.545574E-2	.540129E-2	.29219
3.74726	.505658E-2	.497442E-2	.292267
3.77974	.468957E-2	.459164E-2	.292357
3.8112?	.432914E-2	.426017E-2	.292401
3.84271	.395489E-2	.389755E-2	.292461
3.87419	.364459E-2	.351125E-2	.29?516
3.90567	.329912E-2	.326073E-2	.29256?
3.93715	.304676E-2	.304237E-2	.292617
3.96864	.285557E-2	.280572E-2	.29?654
4.00012	.263299E-2	.252706E-2	.292693
4.0316	.245052E-2	.284996E-2	.292729
4.06308	.224373E-2	.220344E-2	.292765
4.09457	.207249E-2	.203515E-2	.292792
4.12605	.191545E-2	.188093E-2	.292819
4.15753	.177166E-2	.175972E-2	.292844
4.18901	.164005E-2	.161055E-2	.292867
4.2205	.151975E-2	.149343E-2	.292889
4.25198	.140096E-2	.130473E-2	.292908
4.28346	.120975E-2	.118665E-2	.292925
4.31495	.131965E-2	.113713E-2	.292941
4.34643	.113581E-2	.111596E-2	.292956
4.37791	.106073E-2	.104243E-2	.292949
4.40939	.99804E-3	.975025E-3	.29293
4.44088	.932052E-3	.916275E-3	.292941
4.47236	.877442E-3	.862749E-3	.293001
4.50394	.823755E-3	.815062E-3	.293009
4.53532	.735694E-3	.772894E-3	.293017
4.56681	.747971E-3	.745995E-3	.293023
4.59829	.715253E-3	.702906E-3	.293029
4.62977	.687375E-3	.676601E-3	.292034
4.66125	.564104E-3	.653213E-4	.293039
4.69274	.645289E-3	.603955E-3	.293041
4.72422	.630733E-3	.5312E-3	.294044
4.7557	.620503E-4	.611133E-3	.294045
4.79719	.614369E-3	.605121E-3	.293047
4.91867	.612327E-3	.603121E-3	.293047

Run A3

Vapor Temperature	55.8°C	
Sink Temperature	14.0°C	
Gas Content	4.22 std cm^3	
Calculated Heat Transfer Rate	7.00 W	

Axial Position (cm)	T_W^+	T_V^+	Gas Concentration (std cm^3/cm^3)
4.7154?	.959374	1.0	0.0
4.74578	.993545	↓	↓
4.7774	.935449		
4.80995	.957617		
3.84176	.926547		
4.87295	.925505		
4.90432	.923485		
4.93591	.921549		
4.96725	.91932		
4.99578	.914467		
5.03055	.909353	.995	.307024E-2
5.06174	.903032	.992037	.60492?
5.09222	.89513	.987567	.750749E-2
5.12471	.92538	.991024	.115741E-1
5.15619	.873491	.971761	.171472E-1
5.18767	.859202	.959103	.246755E-1
5.21915	.642314	.947463	.344492E-1
5.25054	.822715	.521572	.465903E-1
5.27212	.906404	.595573	.61044?E-1
5.3136	.775504	.868433	.775277E-1
5.34579	.742262	.871598	.956112E-1
5.37157	.71905?	.794361	.11460?
5.40505	.608237	.754557	.13415
5.43953	.556323	.714165	.15342?
5.47102	.613917	.575166	.1720?
5.5065	.591139	.622762	.13375?
5.54342	.553669	.593099	.206261
5.57546	.526772	.55516	.22151
5.59635	.495709	.519005	.235494
5.62943	.465679	.494768	.249264
5.65391	.43602	.452479	.259937
5.68159	.409254	.422114	.270436
5.72283	.392004	.393607	.280125
5.75436	.358101	.366577	.293909
5.79504	.304554	.341532	.296912
5.81752	.312301	.318392	.30423?
5.84831	.291242	.292454	.310915
5.87169	.27164	.275902	.317035
5.91177	.253120	.255702	.322639

Run A3 (continued)

5.94325	.235759	.232757	.327775
5.97474	.219479	.221999	.342459
6.00622	.204234	.206335	.336919
6.0377	.18997	.19172	.40790
6.06918	.176842	.178024	.344456
6.10067	.164169	.155365	.347322
6.13215	.15292	.153507	.350921
6.16363	.141569	.142456	.355775
6.19511	.101534	.132161	.356407
6.2266	.122035	.122572	.358332
6.25808	.11328	.113649	.361068
6.28956	.105077	.105343	.363131
6.32105	.974895E-1	.975171E-1	.365035
6.35253	.903893E-1	.904324E-1	.366781
6.38401	.837175E-1	.937534E-1	.369413
6.41549	.775606E-1	.775466E-1	.36991
6.44698	.718398E-1	.71796E-1	.371290
6.47846	.655229E-1	.664259E-1	.37257
6.50994	.615839E-1	.514946E-1	.373749
6.54142	.569940E-1	.560409E-1	.374852
6.57291	.527349E-1	.525604E-1	.375845
6.60439	.043731	.4359 46E-1	.376774
6.63597	.451187E-1	.449094E-1	.377632
6.66735	.417095E-1	.414975E-1	.378425
6.69884	.355543E-1	.078336	.379157
6.73032	.356294E-1	.354074E-1	.379333
6.7618	.022919	.325955E-1	.380457
6.79328	.304061E-1	.301849E-1	.381014
6.82477	.280288E-1	.278614E-1	.381566
6.85625	.02592	.257117E-1	.382032
6.88773	.243374E-1	.237534E-1	.382511
6.91921	.220957E-1	.210345E-1	.38295
6.9507	.204332E-1	.201230E-1	.38331
6.98218	.189111E-1	.134146E-1	.38367
7.0135	.017252	.171635E-1	.38400
7.04514	.158054E-1	.158230E-1	.38421
7.07662	.147503E-1	.145255E-1	.38454
7.10811	.136101E-1	.134431E-1	.38494
7.14959	.125473E-1	.123957E-1	.38505
7.17107	.115473E-1	.114153E-1	.38523
7.20256	.106619E-1	.105122E-1	.38551
7.23404	.93266E-2	.96905E-2	.38567
7.26552	.905994E-2	.843741E-2	.38595
7.297	.534915E-2	.83239E-2	.38601
7.33849	.768951E-2	.797550E-2	.39618
7.35997	.70553E-2	.697311E-2	.38629
7.39145	.652836E-2	.543775E-2	.386419
7.42294	.501493E-2	.592054E-2	.33653
7.45442	.554216E-2	.545407E-2	.38667

Run A3 (continued)

7.4759	.510643E-2	.502433E-2	.386582
7.51773	.470534E-2	.462975E-2	.386381
7.54237	.435601E-2	.426474E-2	.386901
7.59035	.399605E-2	.392592E-2	.386673
7.61123	.365219E-2	.34217E-2	.387047
7.64341	.339535E-2	.323235E-2	.38711
7.6743	.31306E-2	.307792E-2	.387162
7.70623	.288715E-2	.224832E-2	.387221
7.73776	.255335E-2	.251825E-2	.387271
7.76324	.245769E-2	.241607E-2	.387316
7.80073	.226577E-2	.22304E-2	.387257
7.83381	.209529E-2	.205394E-2	.38743
7.86262	.193607E-2	.190354E-2	.35743
7.89517	.179001E-2	.17601E-2	.387462
7.92626	.165512E-2	.152362E-2	.387491
7.95014	.15434E-2	.150821E-2	.387518
7.95962	.142119E-2	.139501E-2	.387543
8.0211	.131357E-2	.129725E-2	.387565
8.05253	.122477E-2	.120535E-2	.387536
8.08407	.115927E-2	.112134E-2	.387604
8.11555	.105142E-2	.10449E-2	.387621
8.14705	.990692E-3	.975565E-3	.387647
8.17752	.926575E-3	.912671E-3	.387651
8.21	.965565E-3	.855532E-3	.387654
8.24145	.01640E-3	.804672E-3	.387675
8.27295	.769733E-3	.759915E-3	.387639
8.30445	.729071E-3	.717546E-3	.387654
8.33597	.691204E-3	.681782E-3	.387702
8.36741	.659375E-3	.650669E-3	.387709
8.39593	.620559E-3	.622597E-3	.387715
8.43037	.606751E-3	.599144E-3	.387721
8.46186	.537015E-3	.575577E-3	.387725
8.49234	.570898E-3	.563751E-3	.387729
8.52465	.558449E-3	.551554E-3	.387731
8.55621	.549629E-3	.542902E-3	.387733
8.58779	.544362E-3	.537734E-3	.387734
8.61927	.54261E-3	.536016E-3	.387745

Run B1

Vapor Temperature	63.35^{o}C	
Sink Temperature	40.12^{o}C	
Gas Content	4.49 std cm^3	
Calculated Heat Transfer Rate	2.014 W	

Axial Position (cm)	T_W^+	T_V^+	Gas Concentration (std cm3/cm3)
1.53779	.92536	1.0	0.0
1.56541	.925-92		
1.59094	.924593		
1.72347	.924731		
1.75	.923636		
1.73052	.922776		
1.72105	.921605		
1.75153	.920399		
1.34511	.918473		
1.31264	.915101		
1.34817	.912547	.955	.2065955-2
1.9757	.909377	.996965	.2511095-2
2.00423	.904501	.996216	.4043-5-2
2.05476	.599455	.995559	.5552525-2
2.05929	.597001	.931774	.7520466-2
2.09531	.825277	.975617	.1904555-1
2.12634	.095411	.967252	.1322595-1
2.15537	.86537	.959169	.1715915-1
2.1574	.952942	.946395	.021925
2.21792	.940545	.932311	.2755595-1
2.24946	.924294	.91579	.3417575-1
2.27399	.605575	.895763	.0417
2.30952	.73857	.875575	.5011955-1
2.34005	.768569	.851424	.05934J
2.37057	.746414	.825415	.5327735-1
2.4011	.723124	.797524	.7575755-1
2.43165	.699589	.750075	.5075155-1
2.46215	.674319	.727442	.101924
2.49269	.647242	.70599	.113542
2.52422	.620634	.57409	.124535
2.55575	.593969	.642085	.135579
2.52429	.567008	.610231	.14557
2.61451	.540255	.57994	.157128
2.64574	.513903	.545279	.157591
2.57526	.497985	.513457	.177715
2.70549	.452557	.439644	.135573
2.73592	.439031	.461279	.195054
2.75745	.414195	.435239	.203375
2.75792	.39119	.40977	.211599
2.92851	.369059	.395479	.215555

Run B1 (continued)

2.95904	.347845	.352352	.225516
2.03957	.327565	.340405	.242092
2.9501	.302212	.313551	.235121
2.95066	.289723	.299221	.243924
2.98115	.272295	.321203	.249184
3.01168	.25564	.283525	.254189
3.04221	.249864	.246949	.258271
3.07274	.224972	.231252	.263243
3.10327	.210874	.215473	.267339
3.1329	.197553	.202549	.271164
3.16432	.184995	.193444	.274735
3.19445	.173155	.177119	.276072
3.22538	.161997	.165534	.281189
3.25591	.151497	.15445	.284098
3.29644	.141512	.14443	.286615
3.31697	.132334	.134525	.289251
3.3475	.123611	.12554	.291719
3.37303	.11542	.117403	.293929
3.40956	.10773	.109495	.29599
3.43909	.100523	.102097	.297913
3.46962	.093763	.951565E-1	.299702
3.50014	.274232E-1	.396539E-1	.301322
3.53067	.814942E-1	.825753E-1	.302942
3.5612	.759222E-1	.758912E-1	.304395
3.59172	.707204E-1	.715755E-1	.305755
3.62226	.653735E-1	.666067E-1	.307019
3.65278	.061324	.619639E-1	.308199
3.68332	.057071	.576273E-1	.309296
3.71205	.520967E-1	.535781E-1	.310319
3.74432	.493941E-1	.497985E-1	.311272
3.7749	.459173E-1	.462718E-1	.31216
3.80543	.426813E-1	.429322E-1	.312986
3.83595	.395615E-1	.399149E-1	.313755
3.86648	.365446E-1	.370957E-1	.314471
3.89702	.024218	.343915E-1	.315137
3.92755	.317695E-1	.319097E-1	.315756
3.95808	.294273E-1	.295988E-1	.316333
3.93861	.273625E-1	.274475E-1	.316863
4.01914	.253834E-1	.254457E-1	.317345
4.04966	.245411E-1	.235836E-1	.317929
4.03019	.219266E-1	.219513E-1	.318259
4.11072	.202719E-1	.202421E-1	.318559
4.14125	.187497E-1	.187436E-1	.319052
4.17179	.173771E-1	.173566E-1	.319374
4.20231	.160583E-1	.160663E-1	.319492
4.23284	.149525E-1	.148621E-1	.319935
4.26337	.127726E-1	.137564E-1	.320552
4.2939	.127577E-1	.127252E-1	.320517
4.32443	.119152E-1	.117693E-1	.320752

Run B1 (continued)

4.25435	.109325E-1	.108825E-1	.320372
4.38548	.010114	.100512E-1	.351175
4.41601	.995512E-2	.950647E-2	.321362
4.44654	.865306E-2	.859617E-2	.321535
4.47707	.80405E-2	.79444E-2	.321696
4.5076	.712931E-2	.734149E-2	.321944
4.53513	.694072E-2	.684056E-2	.321922
4.54866	.632509E-2	.626682E-2	.352108
4.59919	.554652E-2	.579313E-2	.322225
4.62971	.540931E-2	.535393E-2	.322233
4.66024	.500195E-2	.494877E-2	.322433
4.69077	.452703E-2	.457525E-2	.422525
4.7213	.429154E-2	.423117E-2	.322604
4.75183	.396226E-2	.391443E-2	.322657
4.78236	.357043E-2	.362327E-2	.322759
4.81289	.340124E-2	.335577E-2	.322524
4.84342	.315423E-2	.311036E-2	.322895
4.87395	.296751E-2	.293553E-2	.32294
4.90447	.272054E-2	.267923E-2	.32299
4.935	.255122E-2	.249215E-2	.323037
4.96553	.235969E-2	.232115E-2	.323079
4.94406	.220153E-2	.216581E-2	.323117
5.02659	.205931E-2	.202514E-2	.323151
5.05712	.19316E-2	.193325E-2	.323182
5.03765	.181644E-2	.179433E-2	.32321
5.11818	.171351E-2	.169265E-2	.323235
5.14871	.162245E-2	.159254E-2	.323257
5.17923	.154241E-2	.151343E-2	.323277
5.20976	.147294E-2	.144481E-2	.323294
5.24029	.141361E-2	.133522E-2	.323408
5.27082	.126404E-2	.133728E-2	.32332
5.30135	.133392E-2	.157766E-2	.32333
5.33168	.123297E-2	.126713E-2	.323337
5.36241	.127101E-2	.124545E-2	.323343
5.39294	.125739E-2	.12325E-2	.323346
5.42347	.125055E-2	.12282E-2	.323347

Run B2

Vapor Temperature	67.1°C	
Sink Temperature	40.2°C	
Gas Content	4.421 std cm³	
Calculated Heat Transfer Rate	4.572 W	

Axial Position (cm)	T_W^+	T_V^+	Gas Concentration (std cm³/cm³)
4.36767	.92526	1.0	0.0
4.3934	.925336		
4.42093	.924773		
4.4534	.924125		
4.43922	.92355		
4.53052	.95239		
4.55105	.321167		
4.58159	.915591		
4.61211	.917546		
4.64253	.914277		
4.67715	.911385	.955	.252349E-2
4.70363	.907154	.992779	.973629E-2
4.73425	.903022	.93571	.005591
4.76475	.395917	.995544	.756495E-2
4.79526	.949742	.979935	.104525E-1
4.82531	.979465	.972752	.142029E-1
4.85634	.569022	.963494	.159962E-1
4.32637	.956931	.951915	.242275E-1
4.91734	.942002	.937751	.521425E-1
4.94792	.926950	.920808	.406979E-1
4.97345	.909008	.900591	.506096E-1
5.00359	.78926	.577315	.517953E-1
5.03951	.757715	.852929	.741602E-1
5.07604	.744525	.82503	.875125E-1
5.10057	.71983	.795135	.101551
5.1311	.694013	.76349	.116315
5.16163	.64718	.730634	.121263
5.19215	.539652	.697026	.145261
5.22269	.511695	.667113	.151102
5.25321	.563571	.629295	.175611
5.28374	.555517	.595913	.189551
5.31427	.527745	.563262	.903124
5.3448	.500442	.531545	.215963
5.37533	.473762	.500927	.22913
5.40586	.447929	.471518	.239611
5.43639	.432741	.443326	.250406
5.46691	.379571	.41656	.260532
5.49744	.375367	.391052	.27001
5.52797	.35316	.356359	.27997
5.5595	.321966	.343943	.287145

Run B2 (continued)

5.58903	.31179.	.333271	.294852
5.61956	.292611	.#01935	.#0205
5.65009	.274424	.292459	.308768
5.68062	.257203	.264304	.31502
5.71115	.240918	.24717	.320844
5.74169	.225539	.231049	.325269
5.7722	.211031	.215991	.3#1322
5.80273	.197359	.201649	.336028
5.83325	.184497	.165572	.34041
5.96379	.173377	.175712	.34449
5.59432	.150994	.153942	.34025
5.95485	.150301	.152902	.351328
5.95523	.140253	.142556	.#55132
5.99591	.139645	.132945	.353189
6.01644	.122015	.123791	.361043
6.04696	.113733	.115299	.3627
6.07749	.105938	.107355	.366174
6.10202	.927212E-1	.993257E-1	.366477
6.13355	.913403E-1	.929814E-1	.370619
6.16909	.095598	.864927E-1	.372513
6.17961	.794409E-1	.804#19E-1	.374469
6.22014	.740932E-1	.747729E-1	.376195
6.26067	.689125E-1	.634907E-1	.#77901
6.2912	.05407	.645522E-1	.379295
6.32173	.595493E-1	.539655E-1	.#80694
6.35225	.553209E-1	.555795E-1	.381975
6.38279	.513950E-1	.516946E-1	.383176
6.41331	.477265E-1	.479628E-1	.384293
6.44354	.44#061E-1	.444952E-1	.#8533
6.47437	.411995E-1	.412669E-1	.386295
6.5049	.03815	.033262	.39719
6.53543	.253854E-1	.354559E-1	.393022
6.56596	.329119E-1	.032865	.389795
6.59648	.#04172E-1	.#04465E-1	.#99512
6.52701	.281895E-1	.281983E-1	.3#0178
6.65754	.026116	.281092E-1	.39079#
6.68807	.241323E-1	.241685E-1	.391369
6.7186	.224027E-1	.22356E-1	.391901
6.74913	.207405E-1	.205931E-1	.392234
6.77966	.191953E-1	.191409E-1	.392252
6.81019	.177529E-1	.177001E-1	.393275
6.84072	.164327E-1	.163542E-1	.39#5#2
6.87124	.151356E-1	.151257E-1	.39404#
6.90177	.014054	.139779E-1	.3943##
6.9322	.139929E-1	.129146E-1	.394591
6.96257	.120094E-1	.113297E-1	.3949#
6.99336	.110922E-1	.110179E-1	.395257
7.02389	.1#2543E-1	.101733E-1	.39545#
7.05442	.009472	.933317E-2	.395712

Run B2 (continued)

7.08495	.97493E-3	.96710bE-3	.395934
7.11548	.808091E-2	.200347E-2	.396115
7.14601	.746222E-2	.735649E-2	.396299
7.17653	.689019E-2	.591653E-2	.395456
7.20706	.625176E-2	.62902E-2	.396619
7.23759	.587359E-2	.590435E-2	.396751
7.26512	.543236E-3	.5#5612E-2	.#96892
7.29865	.500693E-2	.484273E-2	.397013
7.32913	.463229E-2	.45617E-2	.397124
7.35971	.426961E-2	.421066E-2	.397325
7.39024	.394377E-2	.393746E-2	.397321
7.42077	.364376E-2	.359006E-3	.397407
7.45129	.3#6774E-2	.331562E-3	.397427
7.49132	.311399E-2	.306539E-2	.39755
7.51235	.268093E-2	.287478E-2	.397627
7.54298	.266709E-2	.26233E-2	.397629
7.57341	.247111E-2	.242961E-2	.397745
7.60394	.229175E-3	.225244E-2	.397797
7.63447	.212786E-2	.20906bE-2	.397844
7.655	.197935E-3	.194314E-2	.397887
7.69552	.18423bE-2	.130397E-3	.397936
7.72605	.171839E-2	.168725E-2	.397962
7.75652	.160718E-2	.157717E-2	.397994
7.78711	.150643E-2	.147798E-2	.398023
7.81764	.141614E-2	.133903E-2	.398049
7.84817	.133556E-2	.1#0971E-2	.398075
7.8787	.126419E-2	.123349E-2	.398092
7.90922	.120157E-2	.117789E-2	.39811
7.93975	.114725E-2	.112449E-2	.398126
7.97029	.110092E-2	.107993E-2	.398139
8.00081	.10622lE-2	.10409E-2	.39815
8.03134	.103092E-2	.101013E-2	.#98159
8.06187	.100679E-2	.996417E-3	.398166
8.0924	.989663E-3	.969594E-3	.398171
8.12293	.979436E-3	.959546E-3	.398174
8.15346	.976034E-3	.956205E-3	.398175

APPENDIX C

LISTING OF COMPUTER CODE FOR 1-DIMENSIONAL
MODEL OF CONDENSATION HEAT TRANSFER IN THE
PRESENCE OF AN INSOLUBLE GAS

NOTE: The "⁂" sign appearing in the printout is a misprint for the numeral "3".

```
1  T
                         06-FEB-76
   LII         W(264),C(264),D(264),P(264)
       FNX1(T)=A4*EXP(C5)*T**A3
       FNPO(T)=A1*EXP(A2/T)*T**A2
10 READ Z0           !TOTAL CONDENSER LENGTH
   DATA 16.
20 READ G1,G2,W1,W2  !G-FILM,G-SINK,K-WALL,A-WALL
   DATA .4126,.02252,.0117,.4202
   READ V1,V2,V3     !A-VAPOR,CONST. IN C*D,HT. OF VAPOR.
26 DATA 1.047,2.81E-9,31000.
25 READ A0,A2,A3     !LN(P)= A0 + A2/T + A3*LN(T)  (P IN ATMOSPHERES)
36 DATA 20.8275,-4344.47,-2.90124
40 READ N,Z2,M       !N=GAS-ZONE INCR.,Z2=DIM. LENGTH,M=INCR. IN FREE Z.
41 DATA 114.,2.5,10.
45 READ E5           !MAX. ERROR PERMITTED IN T-WALL PER ITERATION
46 DATA .001
51 INPUT"T-VAPOR=";T1
52 INPUT'T-SINK=";T3
53 INPUT STD. CC. OF GAS= ;G0
60 H=Z2/N:N1=N+1:N2=N+2:M1=M+1:M2=M+N:M3=M+N+1
65 A1=273.15*E*P(A0):P1=FNX1/T1+273.15/:A4=A1/P1
70 U0=T3+273.15:U9=T1-T3:C5=U9/4.:C3=H**2*G1+W1*W2/G5*V1*V3+/3)
71 C1=SQR(W1*W2/G2):G3=1./(1./G1+1./G2):W3=G3/G2
72 P1=-2.-(1.+G1/G2)*H**2:P2=-G1*H**2/G2
73 H0=Z1*H
80 MAT W=CON(M1)
91 MAT W=(W*)*W
95 V(1)=.995:C(1)=0.:D(1)=W(1)       !ADJUST FOR CALC. OF C(2),D(2)
100 FOR I=2 TO N2
105 V(I)=E*P(-(I-1)*H):W(I+M)=W3*V(I):NEXT I
110 P(2)=1./P1
115 FOR I=3 TO M3    !P-MATRIX FOR WALL TEMP. SOLUTION
120 P(I)=1./(P1-P(I-1)): NEXT I
150 T2=0.: GO TO 260
190 T3=0.
200 FOR I=2 TO N1    !CALC. C AND D MATRIX'S FOR VAPOR TEMP. SOLN.
205 T=U0+U9*V(I):C6=A2/T:Y=A4*EXP(C6)*T**A3:C7=A3-C5
210 G=C5*(V(I+1)-V(I-1))*(C7*(1.-Y)+C6/C7-.5)/T
215 F=C3*SQR(T)*(1./Y-1.)/C7
220 B=-(2.+F)-(1.-G)*C(I-1)
235 C(I)=(1.+G)/B:D(I)=-(F*W(I+1)+(1.-G)*D(I-1))/B
240 NEXT I
250 V(N1)=(F*W(M2)+2.*D(N))/(2.+F+2.*C(N))
260 FOR I=N TO 2 STEP -1  ! VAPOR TEMPERATURE PROFILE
265 V(I)=D(I)-C(I)*V(I+1): NEXT I
280 D(2)=(B2-W3)/P1
285 FOR I=3 TO M     !D MATRIX FOR WALL TEMPERATURE CALCS.
290 D(I)=(P2-D(I-1))*P(I):NEXT I
300 FOR I=M1 TO M2
305 D(I)=(B2*V(I-M)-D(I-1))*P(I):NEXT I
310 W(M3)=(B2*V(N1)-2.*D(M2))/(P1-2.*P(M2)):M4=M2
325 FOR I=M2 TO 2 STEP-1
330 T1=W(I):W(I)=D(I)-P(I)*W(I+1):T2=ABS(T1-W(I))
335 IF T2<T3 GO TO 340
340 T3=T2
345 NEXT I
400 IF T3>E5 GO TO 190
600 C3=(P1-FNP0(U0))/U0:T=U0+U9*V(1):C(1)=(P1-FNP0(T))/T
605 T=U0+U9*V(N1):C(N1)=(P1-FNP0(T))/T
610 G=.5*(C(1)+C(N1)): O2=.5*(W(1)+W(M2))
612 FOR I=2 TO M1  !INTEGRATE HCG AND TEMP. PROFILES
613 O2=O2+W(I): NEXT I
615 FOR I=2 TO N   !INTEGRATE GAS AND TEMP. PROFILES
620 T=U0+U9*V(I): C(I)=(P1-FNP0(T))/T
625 G=G+C(I): O2=O2+W(I+M):NEXT I
630 G=V1*H0*G: O2=U9*G2*H0*O2: Z7=(G0-G)/(V1*C1)
640 Z5=Z0-(Z7+Z2*Z1+H0*M):O1=U9*G2*W(1)*Z5:O3=O1+O2
645 FOR I=1 TO M3
650 D(I)=Z5+H0*(I-1):NEXT I
670 PRINT:PRINT'CONCENTRATION AND TEMPERATURE PROFILES":PRINT
671 PRINT:PRINT O1,O2,O3:PRINT
680 FOR I=1 TO M
690 PRINT D(I),W(I):NEXT I
691 FOR I=M1 TO M2
692 PRINT D(I),W(I),V(I-M),C(I-M):NEXT I
700 FOR I=1 TO N1
710 D(I)=H0*(I-1):NEXT I
720 PRINT:PRINT
730 FOR I=1 TO N1
740 PRINT D(I),W(M+I),V(I),C(I):NEXT I
800 MAT PRINT D(M1),
900 END
```